Ph. D. DISSERTATION

EXPERIMENTAL VERIFICATION OF ION TRANSPORT MECHANISM BY ION CONCENTRATION POLARIZATION AND ITS APPLICATIONS

이온 농도 분극에 의한 이온 수송 기작의 실험적 증명 및 응용

BY

WONSEOK KIM

AUGUST 2017

DEPARTMENT OF
ELECTRICAL AND COMPUTER ENGINEERING
COLLEGE OF ENGINEERING
SEOUL NATIONAL UNIVERSITY

Abstract

EXPERIMENTAL VERIFICATION OF ION TRANSPORT MECHANISM BY ION CONCENTRATION POLARIZATION AND ITS APPLICATIONS

WONSEOK KIM

DEPARTMENT OF
ELECTRICAL AND COMPUTER ENGINEERING
COLLEGE OF ENGINEERING
SEOUL NATIONAL UNIVERSITY

As the ion concentration polarization (ICP) phenomenon has been intensively researched for a decade, the unprecedented demand for the complete picture of ions and analytes distributions near the nanoporous membrane has been strongly arisen not only for fundamental nano-electrokinetic studies but also for engineering applications. While micro/nanofluidic platform has been generally adopted in such research fields, the low throughput (<nL/min) would hinder the direct concentration measurement near the membrane.

In this work, firstly, we suggested a direct concentration profiling method; instead of time-consuming sample collection, the concentration

changes of the prefilled sample in each reservoir were measured. We experimentally metered the individual ion concentrations near the nanoporous membrane and succeeded for precise elucidation on the previously reported ICP purification and preconcentration mechanisms. As a result, ion distributions caused by ICP were classified with 3 regions; one for outside the ion depletion zone (IDZ) at the anodic side, and the other for inside the IDZ at the anodic side where, and the last one for the ion enrichment zone (IEZ) at the cathodic side. Firstly, we discovered that analytes larger than the size of nanopore were completely repelled by the ICP layer, while most of salts were removed from the analyte stream because most of cations were transported through the nanoporous membrane to sustain ICP phenomenon, and most of anions were consumed by electrode reaction for electro-neutrality requirement at the outside IDZ. These combined effects would provide a versatile process named as "desalted analyte preconcentration" which enables the perfect recovery of target analyte and simultaneously, the removal of unnecessary salts. Secondly, we discovered the concentration inversion of lithium and sodium ion inside the IDZ. Since the induced electric field inside the IDZ was highly amplified up to 100,000 V/m scale, hydrated ions in a water solution would be dehydrated so that mobility inversion of lithium and sodium ion occurred. Finally, we confirmed that the 65 % of cation transportation through the nanoporous membrane occurred, so the concentration

amplification ratio would be controlled at the IEZ as well as the concentration depending on the mobility of the individual ions.

Based on the results analyzed above, we proposed two applications: a lossless regenerative ink manufacturing device and a portable continuous purification device for artificial kidney development. Firstly, as the novel concept of ink recycler, we showed that salt ions which causes serious deterioration of inkjet head were desalted (~40 %) and ink molecules were preconcentrated (~200 %) in a single step operation. Therefore, the presenting demonstration based on suggested profiling would be a key operational mechanism of various refinery industry such as drug discovery and chemical industry. Secondly, by utilizing ion transport mechanism near nanoporous membrane, the ICP purifier, for the first time, was applied for a novel continuous peritoneal dialysate recycler. Most of charged hazardous substances were sufficiently removed by conventional ICP mechanisms. Moreover, slightly charged toxic molecule (creatinine) was mostly eliminated through nanoporous membrane, and uncharged toxic molecule (urea) was perfectly decomposed by electrochemical reactions. Based on the combined removal mechanisms confirmed in a micro/nanofluidic platform, for practical applicability, a macro ICP device with 100,000 times increase in water treatment capacity from 0.1 μL/min to 10 mL/min was newly introduced. As a results, we showed that the blood toxin concentration was reduced up to 10 % at the in-vivo test with 4 hours continuous operation. We

would expect significant advances in a quality of life for chronic kidney disease patients by this ICP purifier as a portable dialysate recycler.

Keywords : Micro and nanofluidic device, Nanoelectrokinetics, Ion concentration polarization phenomenon, Ultra micro concentration measurement, Desalted analyte lossless preconcentration, Portable dialysate recycler

Student Number : 2013-30225

Contents

List of Figures

List of Tables

Chapter 1 Introduction

1.1 Background

1.1.1 Ion exchange techniques for small-capacity water treatment

In recent years, there is a growing need for a distributed, small-capacity water treatment system that is low in energy and equipment costs, and does not cause environmental pollution problems. Large desalination plant is difficult to cope with depletion of fossil energy, environmental pollution, and climate change due to high energy and facility cost. However, the distributed small water treatment system can be customized according to environmental factors such as area and season, in addition to desalination technology, it is also applicable to small-capacity systems with various purposes such a dialysate purification for development of artificial kidney. Electrochemical water treatment techniques such as electrodialysis (ED) [1], electrodeionization (EDI) [2], and capacitive deionization (CDI) [3] are the mainstream of the typical small-capacity water treatment technologies. The development background and basic principles of those techniques, and the latest research trends would be introduced. While reverse osmosis technique using short-range interaction characteristics and evaporation technique using phase change characteristics are mainly used in existing large-scale desalination plants, electrochemical small-scale water treatment systems use long-range electrostatic interaction characteristics as shown in Figure 1.1 [4].

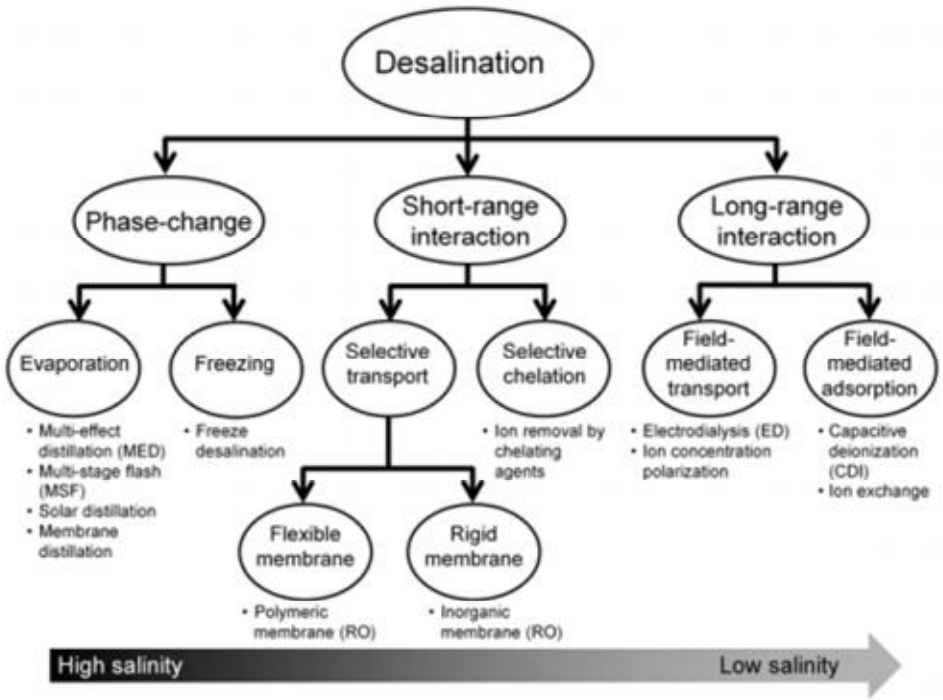

Figure 1.1: Separation mechanisms for desalination technologies [4]. Phase-change and short-range interaction technologies are widely used for desalination of high salinity water such a sea water, but long-range interaction technologies are suitable for desalination of low salinity water such a brackish water or small-scale water treatment system.

A representative example of long-range electrostatic interaction characteristics is the electrophoresis. An ion which has an electrical charge and exists between neutral water molecules is hydrated with water molecules and accelerated by the electric field. Thus, an electric field makes ions be transported to desired location so that depleting or enriching ions within a particular region. The anions move to the anode and the cations to

the cathode so that electric double layer (EDL) is formed because the charged solid such as the surface of fluidic channel and membrane attracts ions with opposite charges. In general, the thickness of the EDL is thinner with higher concentration of ions in the fluid, for example, about 1 μm for deionized water and about 1 nm for seawater. That is, in an area smaller than the thickness of the EDL from the solid surface, an electrostatic environment is formed in which only the electrical charge opposite to the surface charge can exist. [5] Based on this principle, it is possible to selectively adsorb or transfer ions in water using a charged electrode or an ion exchange membrane. This electrochemical water treatment method has advantages of low facility cost and scalability based on a small scale since water treatment can be performed only by an ion selective electrode or a membrane. However, since the energy cost of treating seawater is higher than that of reverse osmosis as shown in Figure 1.2 [6], electrochemical water treatment method is mainly applied to the low salinity level systems such as brackish water desalination plants, food processing, and production of chemicals.

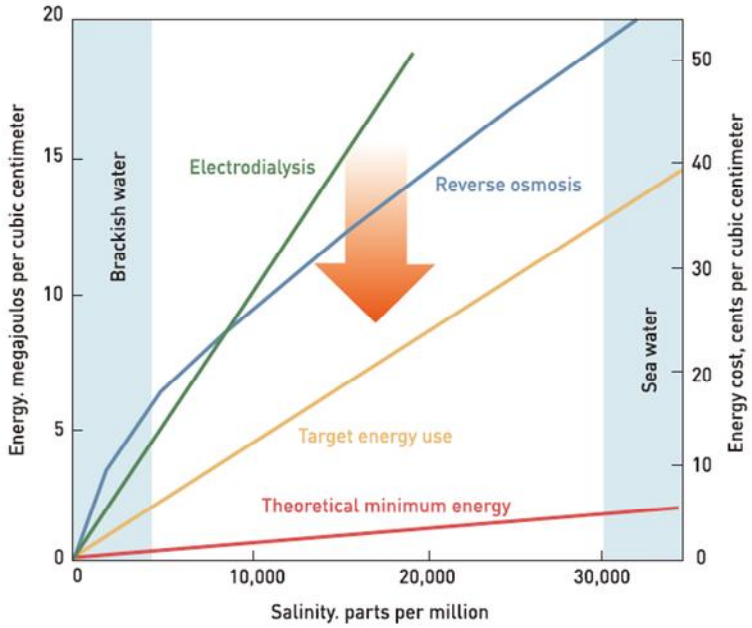

Figure 1.2: Energy cost comparison of reverse osmosis and ED [6]. Since the energy cost of treating seawater (>10,000) is higher than that of reverse osmosis, electrochemical water treatment method is mainly applied to the low salinity level systems (<10,000).

1.1.2 Electrodialysis (ED)

The ED is one of the membrane separation processes using an ion exchange membrane [1]. The ion exchange membrane is fabricated to constitute very small pores below the electric double layer thickness based on the surface charge of the material constituting the membrane. Co-ions that are the same as the surface charge polar cannot pass through the exchange membrane, and only counter-ions that are opposite can pass through the exchange membrane. Depending on the polarity of ions that can pass through the membrane, they are categorized as cation exchange membrane (CEM) which selectively passing only positive ions and anion exchange membrane (AEM) which selectively passing negative ions. The ED device has a configuration in which the two types of ion exchange membranes (CEM and AEM) are arranged in an alternating manner between electrodes at both ends, and a spacer for forming a flow path is arranged between the exchange membranes as shown in Figure 1.3 [7]. Since the ions injected into the spacer channel are moved to the CEM and AEM sides, the supplied salinity water is separated into fresh water and high salinity brine. A single fresh water channel and a single brine channel can be bundled into a unit cell of the ED system and the capacity of the desalination system can be adjusted depending on how many cells are stacked [8].

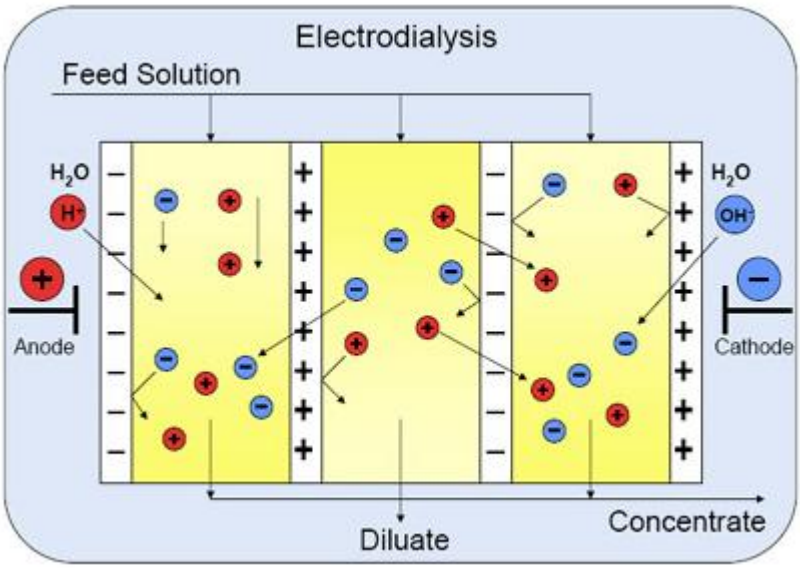

Figure 1.3: Schematic diagram of ED [7]. The ions injected into the spacer channel are moved to the CEM and AEM sides so that the supplied salinity water is separated into fresh water and high salinity brine.

Various researches have been carried out in membrane technologies to increase ion selectivity and electrical driving method to reduce energy consumption, but in sea water desalination field, still high energy cost is shown compared with reverse osmosis method. Therefore, it is mainly applied to the field of brackish water desalination which shows superiority in terms of cost compared with the reverse osmosis method. As a result, nowadays, research is being carried out to secure price competitiveness against reverse osmosis or evaporation by lowering the energy cost of desalination, and to apply it to new commercial processes rather than desalination.

The ED process is considered to be the most viable method among the various electrochemical desalination processes, and the desalination plant is the only process actually operated among them. However, most studies on ED processes have been optimized by monitoring input values (current or voltage, flow rate, salinity) and output values (voltage or current, salinity of fresh water, etc.) without any microscopic approach. This is because microscopic analysis is difficult since ion transport phenomena such as ion concentration polarization (ICP) and electrical vortex occurring in an ED system are complex phenomena caused by multi physics. In recent years, however, ion transport phenomena in ED process have been analyzed through various microscopic approaches based on new visualization systems and state-of-the-art numerical analysis techniques, which would be expected to make the efficient ED process [9-10].

1.1.3 Electrodeionization (EDI)

EDI is designed to fill channels between ion exchange membranes with ion exchange resins to remove salt ions close to 100 %, and these ion exchange resins are configured to act as a kind of ion conductor between the membranes as shown in Figure 1.4 [2, 11].

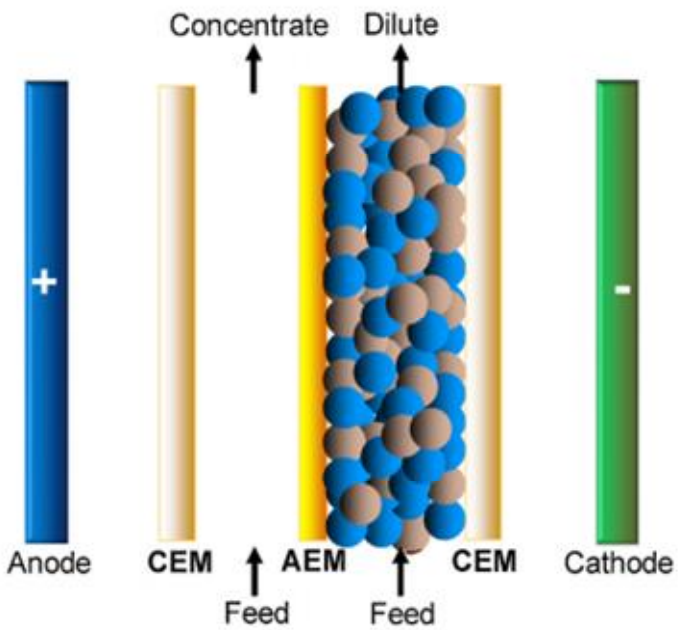

Figure 1.4: Schematic diagram of EDI [2]. The structure is the same as ED device, but ion exchange resins are filled inside the spacer channels so that ion removal ratio is close to 100 %.

The ion-exchange resin is a substance used in the ion exchange process, which exchanges fixed ions on the resin surface with moving ions in the electrolyte and diffuses the absorbed ions in the resin. Due to the ion

exchange resins capable of transferring salinity ions in such electrolytes, it is possible to effectively remove all saline ions, and heavy metal ions or silica having with low charge which have not moved well under an electric field [12-15]. As a result, the maximum ion removal rate can be increased from about 50 % to over 90 % as compared with the ED process.

The EDI process occupies a clear market for ultrapure water production, and practical research has been carried out mainly by the company. Unlike the ED process, it is also noteworthy that various combinations are possible depending on the arrangement of the ion exchange resin, the arrangement of the ion exchange resin and the ion exchange membrane [16-18]. In 2008, Siemens developed a seawater desalination system that combines ED and EDI processes by utilizing the fact that the EDI process has a great advantage in desalinating low-salinity water, proving its price competitiveness compared to the reverse osmosis method [19]. In the future, studies on EDI would be focused on reducing the costs of seawater desalination through various combinations with other systems such as reverse osmosis and ED, rather than an independent platform using only an EDI process.

1.1.4 Capacitive deionization (CDI)

The CDI system consists of a pair of porous electrodes rather than an ion exchange resin. When the electrolyte solution is injected into the channel between the electrodes and the pair of electrodes are charged each positively or negatively at a low voltage of about 1-1.4 V, the positive ions in the solution are electrostatically adsorbed to the negative electrode and the negative ions are electrostatically adsorbed to the positive electrode so that desalination is occur as shown in Figure 1.5 [3, 20]. However, since the amount of ions that the electrode can adsorb is limited, a regeneration process is periodically required to release the adsorbed ions.

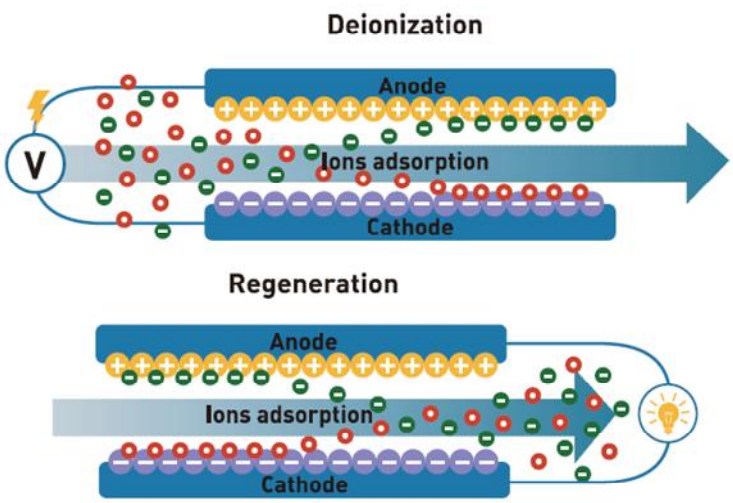

Figure 1.5: Schematic diagram of capacitive deionization (CDI) [20]. The positive ions are electrostatically adsorbed to the negative electrode and the negative ions are to the positive electrode so that desalination is occur.

Compared with ED and EDI processes, the use of electrodes has a disadvantage in structural scalability and a cyclic regeneration. However, with the development of supercapacitors, it has been reported that CDI process has lower energy cost than other electrochemical desalination processes so that many researches have been conducted recently. The cost of energy consumption is lower than other electrochemical desalination process because it can maximize energy efficiency instead of slowly removing salt ions at low drive voltages. Although commercialization has not yet been made on the plant scale, research on increasing the mechanical and chemical stability and lifetime of the porous electrode has been carried out in consideration of commercialization in recent years [21-22].

1.1.5 Ion Concentration Polarization (ICP)

Recently, electrochemical water treatment technology has been combined with micro and nano engineering so that various studies have been carried out from the viewpoints such as development of material and structure of resin, fluid flow analysis under electric field, ion selectivity inside and outside of ion exchange resin [23-24]. Because electrochemical water treatment technology has very high controllability to ions, it is not only to remove salt ions but also has many applications as a flexible platform to treat various kinds of water. One of these approach is the field of nanofluidics. For a last decade, the nanofluidics has been explosively researched about the development of new nanoelectrokinetics fundamentals as well as new engineering applications based on the fundamentals. Especially, a perm-selective ion transportation through a nanostructure has been regarded as a key field of nanofluidics [25-27]. The perm-selectivity (or ion-selectivity) refers an imbalanced ion transportation through the nanostructure (counter-ion more and co-ion less) [5]. The origin of perm-selectivity has been argued until nowadays, since it is impossible to observe directly inside the nanoporous membrane. Theory of electrical double layer (EDL) overlapping is widely-accepted hypothesis among these disputes [27-29]. When the pore size of membrane becomes smaller than Debye length scale, EDL is overlapped inside the pore so that the electrostatic repulsion (or attraction) initiates the perm-selectivity. Only counter-ion can pass

through the membrane and remained co-ions started to be repelled and this phenomenon is accelerated with an applied electric field across the membrane. While the origin of the selectivity has been debated until nowadays such as the overlapped electrical double layer (EDL) [30-32], new fundamentals and novel engineering applications utilizing the perm-selectivity opens several critical research fields. One of most exciting features was ion concentration polarization (ICP) as shown in Figure 1.6 [33].

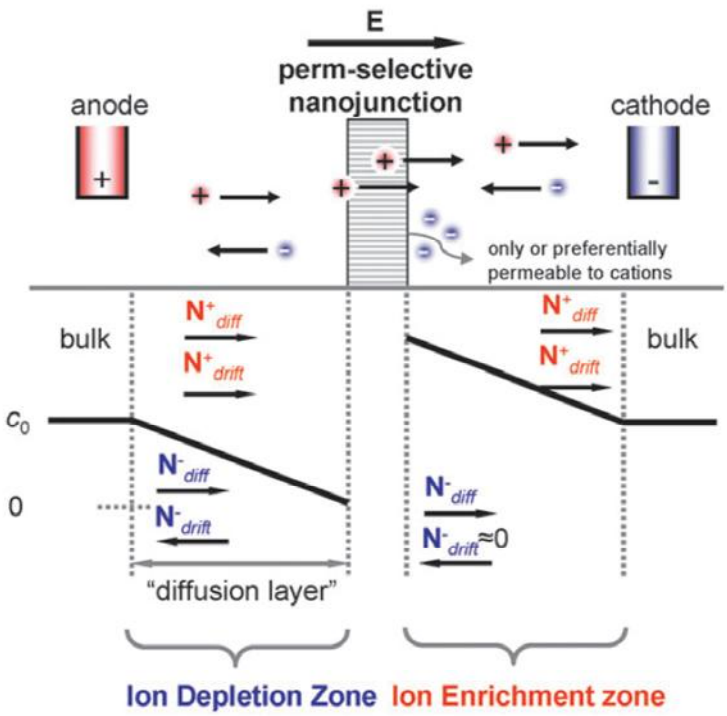

Figure 1.6: Schematic diagram of concentration distribution by ICP phenomenon [33]. Only counter-ion can pass through the membrane and remained co-ions started to be repelled and applied electric field accelerate this phenomenon. N^+ refers the flux of cation and N^- refers the flux of anion.

ICP describes the polarization of ionic concentration near the nanoporous membrane (or nanochannel) under dc bias [34]. Typical behavior is that the concentration largely depleted at the anodic side of membrane and enriched at the cathodic side of membrane. Finally, an ion depletion zone (IDZ) is formed at the anodic side and an ion enrichment zone (IEZ) is formed at the cathodic side in the case of cation-selective membrane.

Although the science behind the ICP such as the source of overlimiting current [34, 35-36] and electrokinetic instability [28-29, 39-43] has been observed, various noble applications have been introduced by using rearranged concentration distributions due to ICP phenomenon as shown in Figure 1.7 [34]. The concept of ICP purifier and preconcentrator has been successfully developed in the form of either batch type [33, 44-50] or continuous type [51-53]. Batch type device shows high concentration amplification factor, but it is challenging to extract the concentrated sample without losing the amplification ratio [45, 46]. These ICP preconcentrators are expected to enhance the detection limit of any sensor for detecting low abundant samples such a biomarkers in a body fluid.

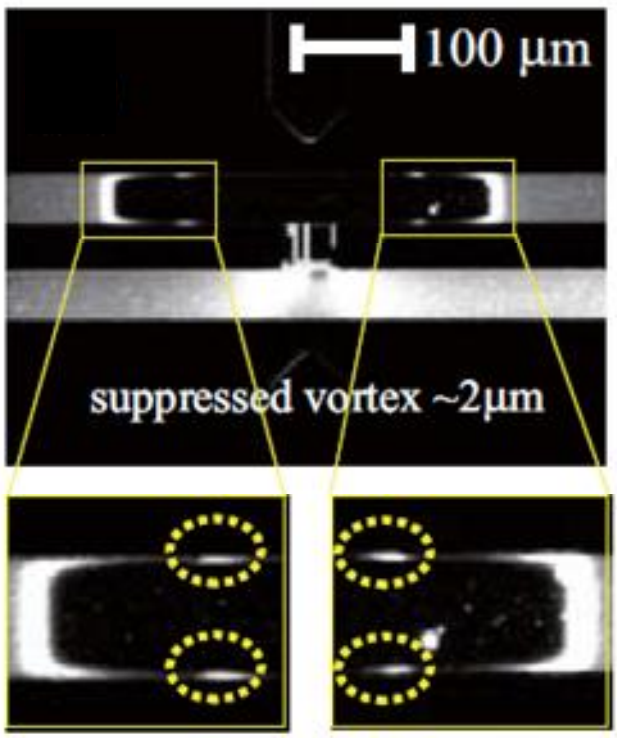

Figure 1.7: Image of batch type device for preconcentration by ICP [34]. Although ICP phenomenon was generated with electrokinetic instability, it showed high concentration amplification factor so called preconcentration.

While continuous type device resolved the extraction problem, it has suffered from a lower preconcentration factor. However, the purification and desalination applications by the continuous extraction of fluid inside the ion depletion zone has been drawn significant attention because this micro and nanofluidic platforms could be developed for a portable device which is essentially useful in remote settings as shown in Figure 1.8 [51]. In the

meantime, one can utilize a brine stream of the purifier as well for developing molecular preconcentrators [33, 51].

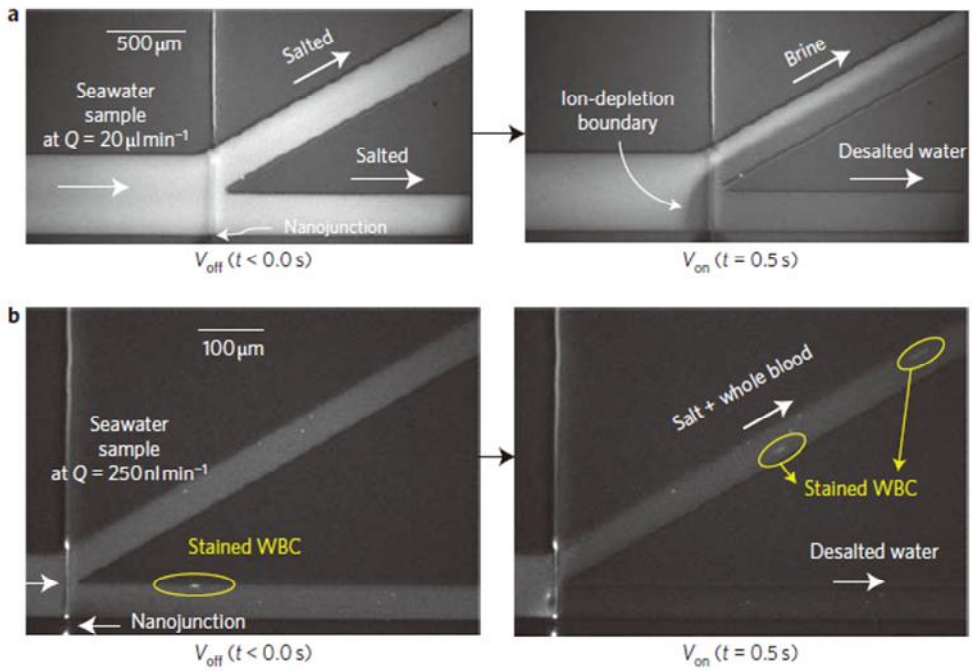

Figure 1.8: Image of continuous type device for desalination by ICP [51]. Seawater sample was injected into the microchannel and started to be separated into brine and desalted streams with applying voltage and flow rate.

Regardless of the advantages and disadvantages of each of the aforementioned device types, both types should be increased of processing capacity for practical applications. Several advantages of micro and

nanofluidic mechanics such as laminar characteristics and gravity independency would be destroyed with scaling up by widening microchannel dimension. Electrokinetic instability becomes severer with larger microchannel dimension [28, 54-59] while it is suppressed and ICP is stably formed in a small dimension microchannel because of surface conduction mechanism [37-38]. However, the dimension of microchannel should be expanded more than millimeter to obtain practical capacity.

1.2 Motivation

Ions are the major carrier of electro-fluidic system and their motions are determined by external conditions such as electric fields, concentration gradients and physical characteristics of the background fluid. Therefore, the complicated sum of drift, diffusion and convection motions results in the final trajectory of ions and the alternation of this basic mechanism conveys a various electrokinetic phenomenon. Especially, nanoscale electrokinetic fundamentals and new applications based on them have been actively investigated along with recent remarkable development in nano-fabrication technologies. As shown in Figure 1.7, the continuous extraction of sample inside the IDZ (white channel) would be utilized as electro-purification device, while the extraction of analyte outside the IDZ (red channel) would be used as continuous preconcentrator. The key mechanism of the applications would be a bursting the ion depletion boundary by regulating an external flow rate and electric field. Similar with the conventional ICP applications, the deterministic factor for the ICP system was the ion flux through the nanojunction and the concentration profile around the nanojunction. However, the exact concentration distributions of ions and analytes near the nanojunction are still argued because theoretical and experimental methods were yet to be developed. It has been reported that both anions and cations were rejected from the IDZ and, however, its direct evidences for individual ions were not reported yet due to the extremely

low-throughput of the micro/nanofluidic device. An array of microelectrodes were installed along the microchannels so that the electric potential drops between each pair of microelectrodes were directly measured, but an unwanted electrode reactions were involved to hinder the exact measurement [39, 60-61].

In this work, we suggested a direct concentration profiling method for extremely low-throughput system (~nL/min). Instead of measuring the sample concentration directly coming out from the reservoir, the concentration changes of prefilled sample in each reservoir were measured. The concentration distributions of individual ion and analyte were reassigned by ICP and each concentration were directly measured outside and inside the IDZ, and the IEZ. Thus, as shown in Figure 1.7, we would figure out how much cations were transported through a nanoporous membrane and anions were consumed by electrode reactions as a driving source to sustain ICP phenomenon and where analyte molecules would flow through. The measurement enabled one to explain the exact mechanism of ICP purification and preconcentration. By using the ion transport mechanism, firstly, we would demonstrate concurrent desalting and preconcentration process without loss of analyte which would be valuable process in refinery industry such as ink recycling and bio-analytical research fields. Secondly, we would propose the continuous type peritoneal dialysate purifier for developing portable artificial kidney.

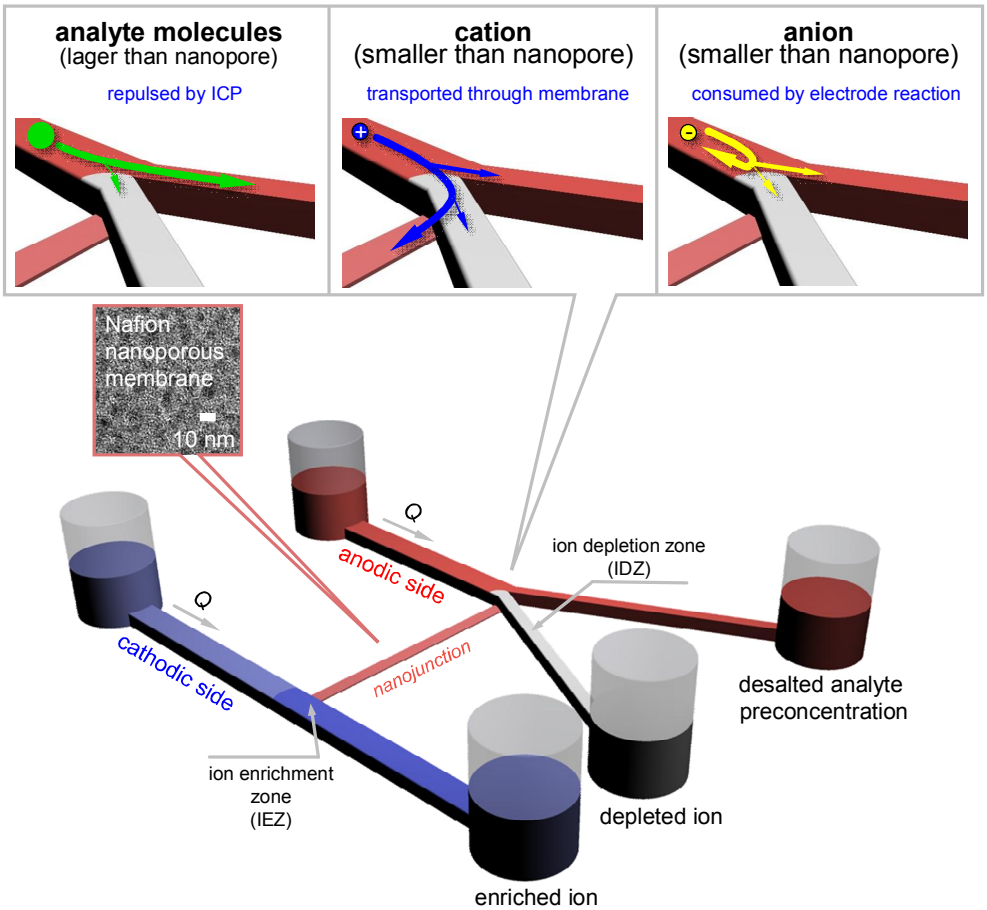

Figure 1.9: Schematic diagram of bifurcated system for ICP operation. Repulsion by ICP and cation flux through the nanojunction caused the rearrangement of concentration distributions at the entrance and the exit of the nanojunction. Nafion [62] was utilized as a nanojunction which had less than 10 nm pore size (See TEM image). Noble concurrent process of "desalted analyte preconcentration" would be expected at the region of the outside ion depletion zone (Red) which was set to be SOI (stream of interest).

1.3 Outline of dissertation

This thesis consists of three Chapters. In Chapter 1, ED, EDI, and CDI, closely related to the ICP phenomenon, would be reviewed, and the background and the value of the ICP phenomenon also would be examined. And the principle of preconcentration and purification due to the ICP phenomenon would be analyzed from the viewpoint of ion migration.

In Chapter 2, we suggested a calculation method to measure individual ion concentration in a micro-nanofluidic platform with extremely low throughput (~ nL/min). Since this measurement method was independent to the factor of dilution, precise measurement would be guaranteed. We discovered new physics due to ion transport by ICP phenomenon from the concentration measurement results by using suggested method. One was "desalted analyte preconcentration" at the outside ion depletion boundary, another was inversion of ion concentration at the inside ion depletion boundary, and the last one was the ion concentration enhancement and modulation at the IEZ zone.

In Chapter 3, as a first application of concentration profiling results in Chapter 2, "desalted analyte preconcentration" process would be applied to the novel concept of ink recycler. We would show how to remove undesirable salts from unrefined ink solution and simultaneously, preconcentrate ink molecules without the loss of them in a single step operation. As a second application, continuous peritoneal dialysate recycler

for portable artificial kidney would be demonstrated. Used peritoneal dialysate contains charged substances such as ions, creatinine and albumin and neutral substance such a urea. Some of ions should be removed and most of body toxins such as creatinine and urea should be removed for dialysate purification. Furthermore, throughput of the micro and nanofluidic device should be highly increased up to 10 mL/min scale for practical utility. Therefore, we would show dialysate purification mechanism by ICP phenomenon and noble concept of macrofluidic ICP device for developing portable artificial kidney. In-vitro and in-vivo used dialysate purification results would be included.

Chapter 2 Ion transport mechanism due to ICP

2.1 Experimental Methods

2.1.1 Concentration measurement method for nano throughput system

We developed a simple but rigorous mathematical formula for calculating individual ion concentrations in extremely low-throughput micro-nanofluidic system. Since the throughput of 20 um width and 15 um depth microchannel for ICP triggering device was 4 nL/min in each, ~250,000 minutes (about 6 months) were needed to collect 1 mL sample which is minimal sample volume for conventional mass spectrometry measurement. Sample loss due to evaporation in such long time would also be challenging to be overcome. Instead of direct measuring the sample coming out from the reservoir, we measured the concentration changes in a prefilled sample solution at each reservoir as described in Figure 2.1. The prefilled sample solution was consisted of D.I. water and background electrolyte ion (BGE_i) that were not participated in any reaction occurred in a microchannel. From these initial and final concentration values at each reservoir, we were able to calculate the concentration of individual ion toward each branch by following simple mathematical derivation.

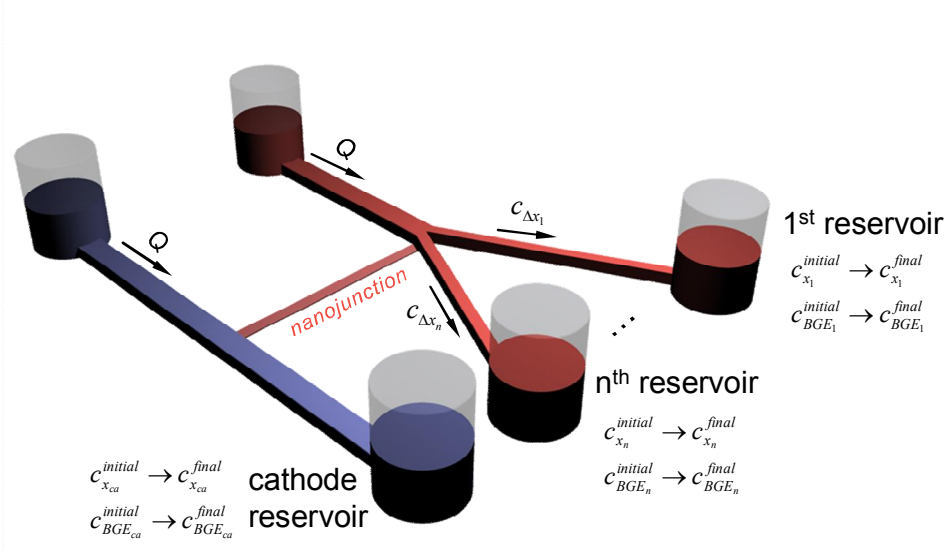

$$c_{\Delta x_i} = \frac{\Delta x_i}{\Delta V_i} = \left(\frac{c_{x_i}^{final} c_{BGE\_i}^{initial} - c_{x_i}^{initial} c_{BGE\_i}^{final}}{c_{BGE\_i}^{initial} - c_{BGE\_i}^{final}} \right), i = 1,2,...,n$$

$$c_{\Delta x_{ca}} = \frac{\Delta x_{ca}}{\Delta V_{ca}} = \left(\frac{c_{x_{ca}}^{final} c_{BGE\_ca}^{initial} - c_{x_{ca}}^{initial} c_{BGE\_ca}^{final}}{c_{BGE\_ca}^{initial} - c_{BGE\_ca}^{final}} \right), ca = \text{cathode}$$

Figure 2.1: Mathematical formula for calculating concentrations of individual ion in extremely low-throughput system. BGE (background electrolyte) was prefilled in each reservoir and concentration change of initial and final BGE and injected ions would be measured to calculate reassigned concentration toward n^{th} reservoir ($c_{\Delta x_n}$). This formula make possible to measure the individual ion concentration within very short time and is independent from dilution factor.

Measured initial and final concentration values of background electrolyte ion at i^{th} branch ($c_{BGE\_i}^{initial}$ and $c_{BGE\_i}^{final}$) would be expressed as

equation (1) and (2); where $BGE_i^{initial}$ and BGE_i^{final} were the mass of background electrolyte at i^{th} reservoir and V_i and ΔV_i were the volume and the incremental volume of prefilled solution at i^{th} reservoir.

$$c_{BGE\_i}^{initial} = \frac{BGE_i^{initial}}{V_i} \tag{1}$$

$$c_{BGE\_i}^{final} = \frac{BGE_i^{final}}{V_i + \Delta V_i} \tag{2}$$

Since the value of $BGE_i^{initial}$ was not changing during a device operation, $BGE_i^{initial}$ / BGE_i^{final} are keep to be 1. Therefore, by dividing eq. (1) to eq. (2), the initial volume V_i per total changed volume ΔV_i at i^{th} branch was given by eq. (3);

$$\frac{V_i}{\Delta V_i} = \frac{c_{BGE\_i}^{final}}{c_{BGE\_i}^{initial} - c_{BGE\_i}^{final}} \tag{3}$$

Since the mass change of target ionic species (Δx_i) and the volume change (ΔV_i) were altered during the time of collecting samples at the each reservoirs, the initial and final concentration of target ionic species ($c_{xi}^{initial}$ and c_{xi}^{final}) at i^{th} branch would be expressed as eq. (4) and eq. (5);

$$c_{x_i}^{initial} = \frac{x_i}{V_i} \quad \text{and} \tag{4}$$

$$c_{x_i}^{final} = \frac{x_i + \Delta x_i}{V_i + \Delta V_i}. \tag{5}$$

Using the method of substitution, the mass of target ionic species (x_i) was eliminated from eq. (4) and (5). Since $c_{x_i}^{initial}$ and $c_{x_i}^{final}$ were obtained under the consideration of prefilled sample volume, the concentration of ion ($c_{\Delta x_i}$) that actually flew through the i^{th} branch was extracted as eq. (6);

$$c_{\Delta x_i} = \frac{\Delta x_i}{\Delta V_i} = c_{x_i}^{final}\left(\frac{V_i + \Delta V_i}{\Delta V_i}\right) - c_{x_i}^{initial}\left(\frac{V_i}{\Delta V_i}\right). \quad (6)$$

Substitute eq. (3) into eq. (6) led to the final eq. (7) for the concentration of ion ($c_{\Delta x_i}$) at i^{th} branch utilizing only $c_{x_i}^{initial}$, $c_{x_i}^{final}$, $c_{BGE\_i}^{initial}$ and $c_{BGE\_i}^{final}$ which were measurable values.

$$c_{\Delta x_i} = \frac{\Delta x_i}{\Delta V_i} = \left(\frac{c_{x_i}^{final} c_{BGE\_i}^{initial} - c_{x_i}^{initial} c_{BGE\_i}^{final}}{c_{BGE\_i}^{initial} - c_{BGE\_i}^{final}}\right), \quad (7)$$
$$i = 1,2,...,n.$$

Concentration variation in cathodic side was also calculated by the same calculation strategy above as eq. (8).

$$c_{\Delta x_{ca}} = \frac{\Delta x_{ca}}{\Delta V_{ca}} = \left(\frac{c_{x_{ca}}^{final} c_{BGE\_ca}^{initial} - c_{x_{ca}}^{initial} c_{BGE\_ca}^{final}}{c_{BGE\_ca}^{initial} - c_{BGE\_ca}^{final}}\right), \quad (8)$$
$$ca = \text{cathode}.$$

From this strategy, the drawback of low-throughput has been resolved and the precise concentration profiles of each ion would be obtained. Furthermore, note that error caused by dilution would be ignored because the value of V_i was erased by the calculation. The operation time should be chosen under the consideration of limit-of-detection of analyzer. In this

work, 10 uL of BGE was prefilled in each reservoir (the evaporation was prevented by covering the reservoirs) and the sample was flowing toward the outlet reservoir for an hour at 4 nL/min.

2.1.2 Fabrication

The micro/nanofluidic device, consisted of anodic multiple branched microchannel and cathodic single branched microchannel was fabricated as shown in Figure 2.2.

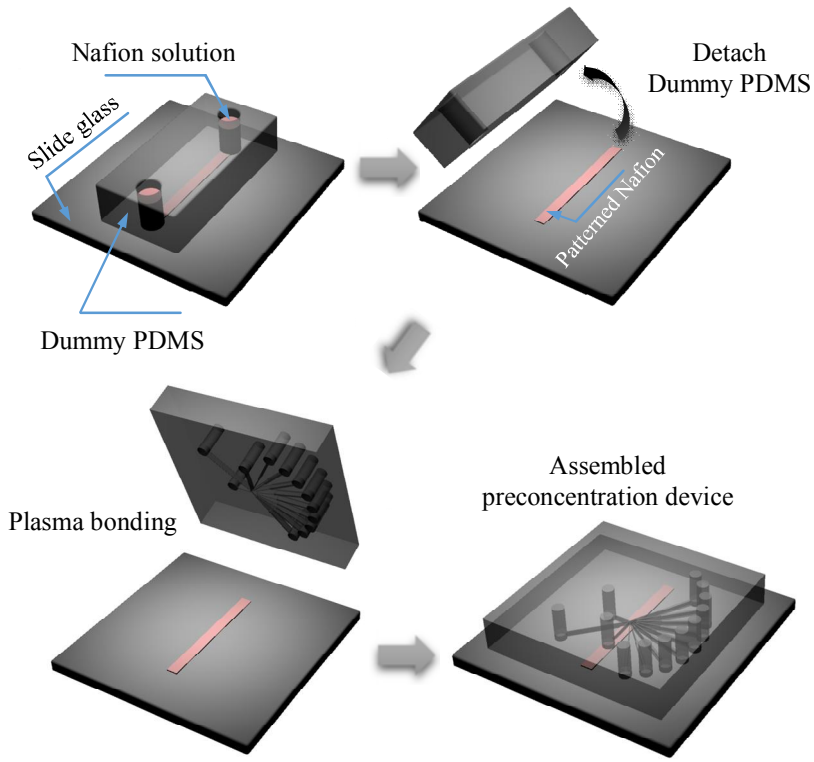

Figure 2.2: Fabrication step of micro/nanofluidic device [63], [64]. Nafion nanoporous membrane was aligned between anodic multiple branched microchannel and cathodic single branched microchannel.

The microchannels were connected each other with nanojunction. As a building block of the microchannels, polydimethyl siloxane (PDMS,

Sylgard 184 Silicone elastomer kit, Dow Corning) was used. A pre-polymer and curing agent were mixed with ratio of 10:1 and bubbles were removed in a vacuum chamber for an hour. Pouring the polymer solution onto the prepared master which had patterned microchannels, and curing in an oven for 4 hours at 75^{o}C. Both the anodic and the cathodic microchannels had the dimension of 20 (branched portion) ~ 200 um (inlet and outlet) width and 15 um depth. Nafion solution (20 w.t.% resin, Sigma Aldrich) was utilized as a cationic perm-selective nanoporous material and we followed surface patterning method was employed to pattern the nanojunction. Firstly, a PDMS block which had a straight microchannel with dimension of 10 mm length, 50 um (9-branched device) or 200 um (2-branched device) width, and 50 um depth was reversibly attached onto a slide glass and Nafion solution was injected into the microchannel by a negative pressure. Secondly, the PDMS block was removed and the slide glass which had straightly patterned Nafion was heated at 95 ^{o}C for 5 minutes to remove solvent from Nafion solution by evaporation. Then only a solid Nafion polymer was remained on the slide glass, and we obtained a flat edge of the nanojunction by cutting the middle of the solid Nafion polymer. Finally, prepared PDMS block which had the anodic and the cathodic microchannels and the slide glass which had the solid Nafion nanoporous membrane were accurately aligned at the bifurcated point using a microscope and chemically bonded together using a plasma bonder (Cute-MP, Femto Science, Korea). The assembled micro/nanofluidic device was shown in Figure 2.3, and the

magnified image was shown in Figure 2.4.

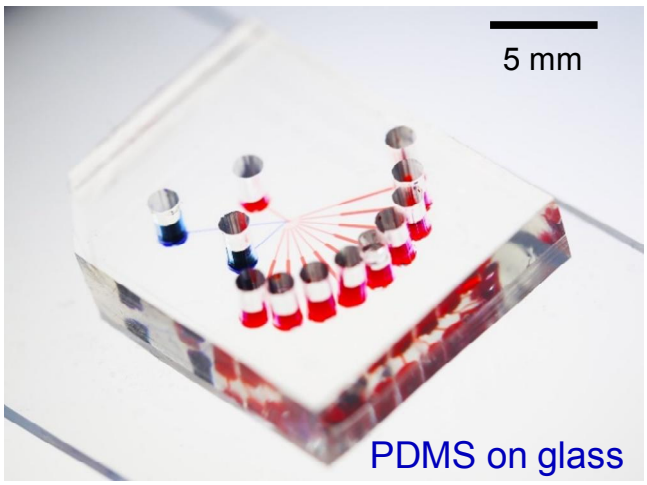

Figure 2.3: Image of fabricated micro/nanofluidic device. Polymeric material, PDMS was used for the microchannel and Nafion nanoporous membrane was used for the nanojunction.

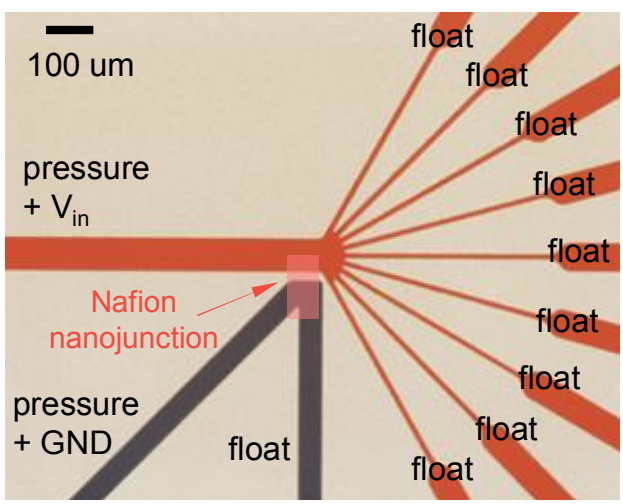

Figure 2.4: A microscope image of the 9-branched device. External pressure and voltage configuration was depicted.

2.1.3 Materials and reagents

Electrolyte solution of LiCl and NaCl (20 ~ 50 mM) mixed with fluorescent dye (Alexa 488, Invitrogen, USA) was used for the anodic side concentration profiling experiment (Chapter 2.2.1, 2.2.2, 2.2.3, 2.2.4), and $MgCl_2$ (50 mM) was used for the cathodic side concentration profiling experiment (Chapter 2.2.2). Note that KCl solution (40 ~ 100 mM) was used as a prefilled solution (background electrolyte in each outlet reservoir). Additionally, negatively charged carboxylated micro-particles (d = 1 um, Invitrogen, USA) was employed to track the flow field.

2.1.4 Experiment apparatus

Both external voltage sources and pressure sources were required to initiate asymmetric ion depletion boundary generation. An external voltage was applied across the nanojunction using a source measurement unit (SMU 238, Keithley, USA). The analyte and buffer solution was injected into the microchannel using a syringe pump (PHD 2000, Harvard apparatus, USA). An inverted fluorescence microscope (IX-51, Olympus, Japan) and a CCD camera (DP73, Olympus, Japan) were used to detect and image the electrokinetic flow in the microchannel. Commercial software (CellSense, Olympus) was used to synchronize the CCD camera with the microscope and to analyze the images. The experimental apparatuses are shown in Figure 2.5.

The electrolyte concentrations of collected cations were analyzed by inductively coupled plasma optical emission spectrometer (iCAP 7400 Duo, Thermo Scientific, USA) or inductively coupled plasma mass spectrometer (Varian 820-MS, Varian, Australia), and both cations and anions were analyzed by ion chromatography (ICS-3000, Dionex, USA). The concentration profiles of fluorescent and ink molecules were analyzed by CellSense program.

Figure 2.5: Experiment apparatus for external sources and imaging process. An external voltage was applied using a source measurement unit (SMU 238, Keithley, USA). The electrolyte solution was injected into the microchannel using a syringe pump (PHD 2000, Harvard apparatus, USA). An inverted fluorescence microscope (IX-51, Olympus, Japan) and a CCD camera (DP73, Olympus, Japan) were used to image the electrokinetic flow in the microchannel. Commercial software (CellSense, Olympus) was used to synchronize the CCD camera with the microscope and to analyze the images.

2.2 Concentration profiles of ions and analytes

2.2.1 Reassigned ion distributions by ICP

With an external constant flow rate (Q) and an electric field ($\mathbf{E}$) in a microchannel without any nano-structure, the total effective force on particle $\mathbf{F}_{particle}$ in microchannel was expressed $\mathbf{F}_{particle} = \mathbf{F}_{elec} + \mathbf{F}_{drag}$ ($\mathbf{F}_{elec}=\mu_{EP}\mathbf{E}$; μ_{EP}: electrophoretic mobility, $\mathbf{E}$: applied electric field and $\mathbf{F}_{drag}= -6\ \pi\mu\mathbf{U}a$; $\mathbf{U}$: flow velocity, μ: viscosity, a: radius of particle). However, with the electric field applied across the nanojunction between anodic and cathodic microchannel, the perm-selectivity of nanojunction derives the electrical repulsive force ($\mathbf{F}_{ICP}$) on particles at the anodic side of nanojunction. $\mathbf{F}_{ICP}$ become weaker as far from the nanojunction. Therefore, the trajectory of particle in micro-nanochannel hybrid device can be expressed by resultant force of $\mathbf{F}_{particle}(y) + \mathbf{F}_{ICP}(y) \equiv \mathbf{F}_{tot}(y)$. Here, y is vertical coordinate from the intersection of the anodic side microchannel and the nanojunction and the both forces can be defined as a function of y. For example, the ion depletion boundary was formed at the location where $\mathbf{F}_{tot}(y)=0$. Therefore, we can largely classify 3 regions with ICP formation; one for inside the IDZ at the anodic side where $\mathbf{F}_{tot}(y)<0$, and the other for outside the IDZ at the anodic side where $\mathbf{F}_{tot}(y)>0$, and the last one for the IEZ at the cathodic side.

As shown in Figure 2.6, ICP was fully developed with 9-branched device at V = 30 V and Q = 40 nL/min to the anodic side microchannel, and

V = 0 V and Q = 40 nL/min to the cathodic side microchannel. These external conditions induced an asymmetric ion depletion boundary due to the different resultant forces in each branch.

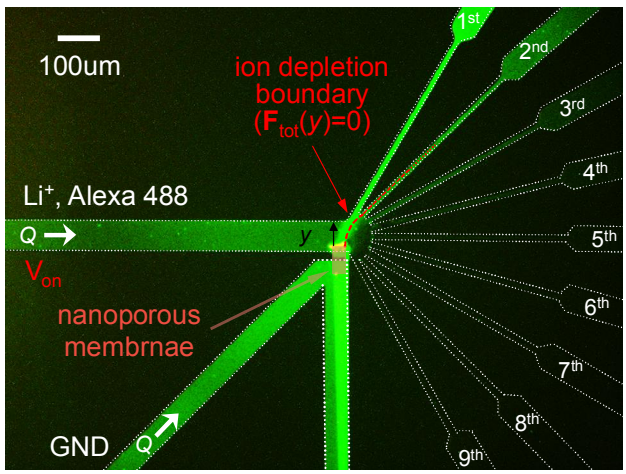

Figure 2.6: Bursting ion depletion boundary in 9-branched device. LiCl (20 mM), NaCl(20 mM), fluorescent (Alexa 488) and 1 um microparticles were injected into the device to analyze individual trajectory of ion and dye molecule caused by ICP.

As shown in 2.7, we expected that the ion depletion boundary was formed between 1st and 2nd branch from fluorescent intensity profiles inside the anodic side microchannel. Most of fluorescent molecules were highly concentrated at 1st branch and slightly concentrated at 2nd branch, while rest of branches were depleted (3rd to 9th branch).

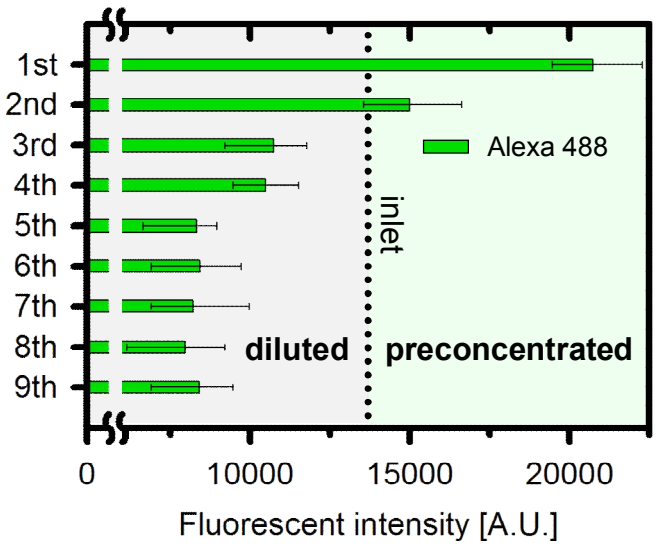

Figure 2.7: Concentration profiling result of fluorescent dye. The concentration factors of fluorescent dye was enhanced at 1st and 2nd reservoirs since the ion depletion boundary was expected to be formed between 1st and 2nd reservoirs.

After an hour operation, samples were collected from 1st to 9th outlet reservoirs in the anodic side microchannel, and the concentration of representing cation, Li^+ was measured and calculated according to eq. (7) to determine the change in concentration value in each reservoir. Similar to previous studies, the concentration inside IDZ (2nd to 9th microchannel) was kept less than 25 % compared to infused inlet concentration as shown in Figure 2.8 so that the electro-desalination process was achieved. See table

2.1, 2.2 and 2.3 to verify the calculation process. (Li^+ was measured and calculated in this experiment because of its high limit of detection.)

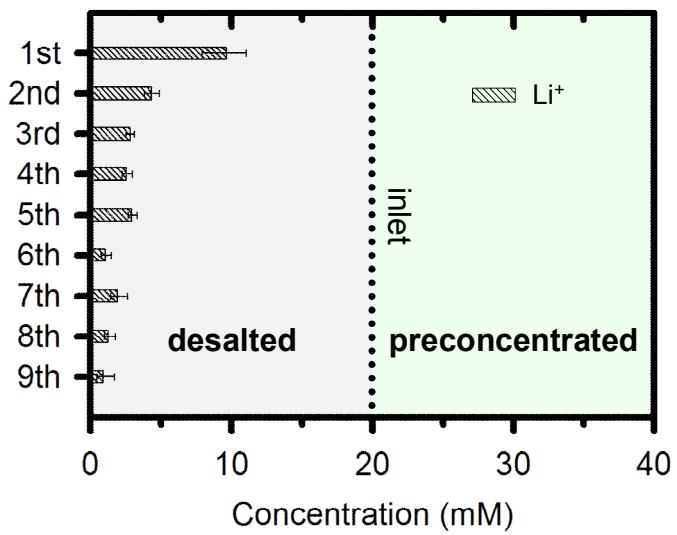

Figure 2.8: Concentration profiling result of Li^+ ion. The concentration factors for the inlet concentration of Li^+ was kept approximately 50 % of inlet concentration in all of branches at the anodic side.

Even though the concentration of Li^+ at 1st branch was the highest (almost twice higher than one from the 2nd to 9th branches), the concentration at the outside IDZ (1st branch) was kept approximately 50 % compared to the inlet concentration. It meant that all of the branches in the anodic side were being desalted regardless of the location of the ion

depletion boundary. The mechanism of ion desalting and dye preconcentration would be concretely analyzed in a following section.

Measured concentration (mM) of Li^+ (analyte electrolyte)		
i^{th} branch	$c_{Li_i}^{initial}$	$c_{Li_i}^{final}$
1	0.216	1.730
2	0.216	1.298
3	0.108	0.865
4	0.216	0.692
5	0.216	0.865
6	0.216	0.346
7	0.432	0.692
8	0.325	0.519
9	0.541	0.519

Table 2.1: Measured initial and final analyte ion (Li^+) concentration of each outlet reservoir in 9-branched device. This values were measured to calculate the absolute changed quantity of analyte ion at each outlet reservoir.

Measured concentration (mM) of K^+ (background electrolyte)		
i^{th} branch	$c_{BGE\_i}^{initial}$	$c_{BGE\_i}^{final}$
1	38.008	32.066
2	38.008	27.943
3	37.931	27.441
4	40.583	31.190
5	40.737	30.037
6	41.755	32.112
7	42.389	31.252
8	40.718	28.763
9	42.063	29.531

Table 2.2: Measured initial and final background electrolyte ion (K^+) concentration of each outlet reservoir in 9-branched device. This values were measured to calculate a quantity of inflow at each outlet reservoir.

Reassigned concentration (mM) of Li^+	
i^{th} branch	$c_{\Delta x_i}$
1	9.902
2	4.300
3	2.845
4	2.272
5	2.685
6	0.778
7	1.420
8	0.987
9	0.467
inlet	19.908

Table 2.3: Reassigned concentration of analyte ion (Li^+) caused by ICP. The values were calculated from eq. (7).

2.2.2 Desalted analyte preconcentration at the outside ion depletion zone

Here we utilized a 2-branched device to create a single stream of outside and inside IDZ, respectively based on the concentration profiling results of Figure 2.8. Figure 2.9 showed the normalized concentration profiles of each ions (Li^+, Na^+ and Cl^-) and dye molecules (Acid Red 52 and Alexa 488) from Q_{SOI}. The value of measured concentration was normalized by that of the inlet concentration.

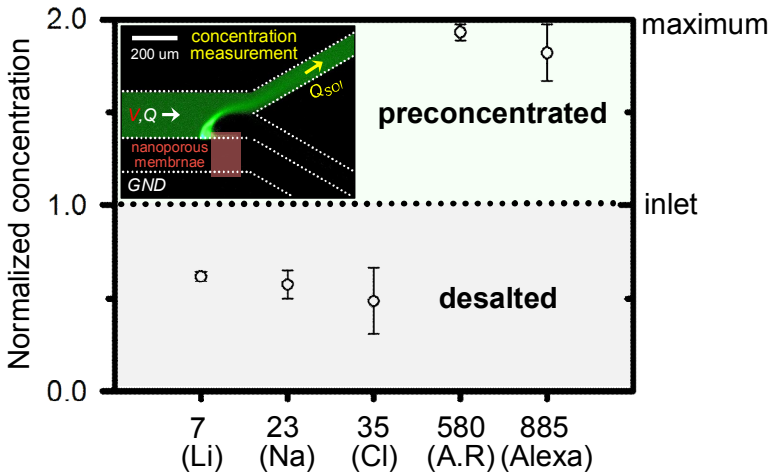

Figure 2.9: Normalized concentration of ions (Li^+, Na^+ and Cl^-) and dye molecules (Acid Red 52 and Alexa 488) at the outside IDZ. 2-branched device was utilized to generate single passage of SOI. While dye molecules were preconcentrated at the SOI, ions were desalted since molecular weight and size of them were much less than the pore size of Nafion nanoporous membrane.

Cations (Li^+, Na^+) were not preconcentrated but desalted as Figure 2.9 and anion (Cl^-) was also found not to be preconcentrated but desalted like cations. This result implied that ions were significantly transported to the other external regions of the SOI, regardless of their polarity. On the other hand, dye molecules were preconcentrated close to the maximum concentration at the SOI. Their losses were expected to be mostly due to photobleaching because they were undetected in the other external regions of the SOI.

For the simplicity, we calculated the number of species (Alexa 488, Li^+, Cl^-) by eq. (3) and eq. (6) to intuitionally understand the physics of molecules and ions transportation due to ICP phenomenon as shown in Figure 2.10. See table 2.4, 2.5, 2.6, 2.7 and 2.8 to verify the calculation process.

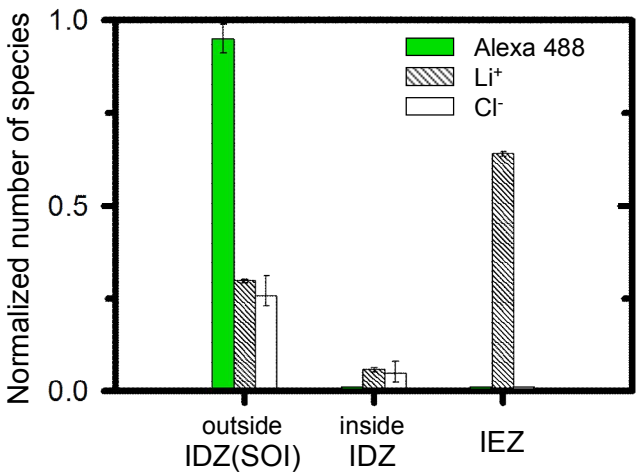

Figure 2.10: Normalized number of collected ions (Li^+ and Cl^-) and dye molecules (Alexa 488) at the outside and inside IDZ and IEZ. The coexistent stream of preconcentrated dye molecules and desalted ions were collected at the outside IDZ (SOI) since ~65 % of cations were transported to IEZ.

Note that approximately 65 % of cation (Li^+ and Na^+) were transported across the nanojunction (from anodic to cathodic) so that both outside and inside IDZ were highly desalted. Their concentration at the cathodic side microchannel was increased over than 120 %. The ratio of amplification at the cathodic microchannel can be adjusted by modulating Q in the cathodic side microchannel. This evidence meant that strong cation flux through the nanojunction was flowing for the development of ICP phenomenon. However, while it had been known that the most of anions (Cl^- in this work) were rejected by the IDZ as well, they were absent at the cathodic side

reservoir but collected at the anodic side reservoir as much as the electro-neutrality condition was satisfied and most of them were consumed by electrode reactions. These experimental verifications would be the key evidences to finalize the argument for the trajectory of ions caused by ICP.

On the other hand, any dye molecules (Alexa 488) were undetected at the region of IEZ. This implied that dye molecules which had heavier weight than ions were transported only toward the SOI, since the size of molecules was larger than the pore size of the nanojunction.

Measured concentration (mM) of Li^+, Na^+, Cl^- (analyte electrolyte)			
x	Li^+	Na^+	Cl^-
c_x^{inlet}	55.828	63.0757	114.786
$c_{x_i}^{initial}$	0	1.229	109.402
$c_{x_1}^{final}$ (outside_IDZ)	7.528	8.891	102.164
$c_{x_2}^{final}$ (inside_IDZ)	1.664	2.740	86.733
$c_{x_3}^{final}$ (IEZ)	14.868	18.933	125.791

Table 2.4: Measured initial and final analyte ions (Li^+, Na^+, Cl^-) concentration of each outlet reservoir in 2-branched device. These were measured to calculate the change of analyte ions at each outlet reservoir.

Measured concentration (mM) of K^+ (background electrolyte)	
x	K^+
c_x^{inlet}	0
$c_{BGE\_i}^{initial}$	106.345
$c_{BGE\_1}^{final}$ (outside_IDZ)	78.144
$c_{BGE\_2}^{final}$ (inside_IDZ)	72.383
$c_{BGE\_3}^{final}$ (IEZ)	71.667

Table 2.5: Measured initial and final background electrolyte ion (K^+) concentration of each outlet reservoir in 2-branched device. This values were measured to calculate a quantity of inflow at each outlet reservoir.

Reassigned concentration (mM)			
x	Li^+	Na^+	Cl^-
$c_{\Delta x_1}$ *(outside_IDZ)*	34.542	36.385	76.192
$c_{\Delta x_2}$ *(inside_IDZ)*	7.634	8.164	5.388
$c_{\Delta x_3}$ *(IEZ)*	68.219	82.461	0

Table 2.6: Reassigned concentration of analyte ions (Li^+, Na^+, Cl^-) caused by ICP. The values were calculated from eq. (7).

Normalized concentration			
x	Li^+	Na^+	Cl^-
$\frac{c_{\Delta x_1}}{c_x^{inlet}}$	0.619	0.577	0.664
$\frac{c_{\Delta x_2}}{c_x^{inlet}}$	0.137	0.129	0.047
$\frac{c_{\Delta x_3}}{c_x^{inlet}}$	1.222	1.307	0

Table 2.7: Normalized concentration of analyte ions (Li^+, Na^+, Cl^-). The values from table 2.6 were normalized by infused inlet concentration of each component.

We could calculate normalized volume change in outlet reservoirs from eq. (3). Normalized volume change in i^{th} reservoir would be expressed as the division of i^{th} volume change (ΔV_i) and total volume change ($\sum_k \Delta V_k$). Then, normalized number of analyte ion ($N_{\Delta x_i}$) would be calculated from the product of normalized concentration ($\frac{c_{\Delta x_i}}{c_{x_i}^{inlet}}$) and normalized volume change ($\frac{\frac{\Delta V_i}{V_i}}{\sum_k \frac{\Delta V_k}{V_k}}$). The formula was expressed as eq. (9).

$$N_{\Delta x_i} = \frac{c_{\Delta x_i}}{c_{x_i}^{inlet}} \times \frac{\frac{\Delta V_i}{V_i}}{\sum_k \frac{\Delta V_k}{V_k}} \tag{9}$$

	Normalized volume change	**Normalized number of Li^+**	**Normalized number of Na^+**	**Normalized number of Cl^-**
i^{th} branch	$\frac{\frac{\Delta V_i}{V_i}}{\sum_k \frac{\Delta V_k}{V_k}}$	$N_{\Delta Li_i}$	$N_{\Delta Na_i}$	$N_{\Delta Cl_i}$
1 (outside_IDZ)	0.435	0.291	0.271	0.312
2 (inside_IDZ)	0.565	0.064	0.061	0.022
3 (IEZ)	0	0.644	0.668	0

Table 2.8: Calculated values of normalized number of analyte ions (Li^+, Na^+, Cl^-) at i^{th} branch. The form of normalized volume change was calculated from eq. (3). The values were depicted in Figure 2.10.

Based on the above experimental measurements, the complete picture of charged species distribution in the 2-branched due to ICP phenomenon was shown in Figure 2.11. In this schematics, the number of cation (n_0^+), anion (n_0^-), and analytes (n_0^a) were initially injected from the anodic side microchannel. As predicted by previous studies, most of charged species regardless of their polarity and size were rejected in the purified channel (gray) so that only ~5 % of both n_0^+ and n_0^- were detected without any analyte molecules. Analytes larger than pore size of the membrane were

rerouted their path toward the upper channel (red) regardless of their polarity so that they were preconcentrated and, remarkably, only ~30 % of initial number of ions were detected at an outlet reservoir of the SOI. Therefore, we would successfully collect all of analytes without the accumulation of ions from the upper channel (red). This concurrent process was named as "desalted analyte preconcentration".

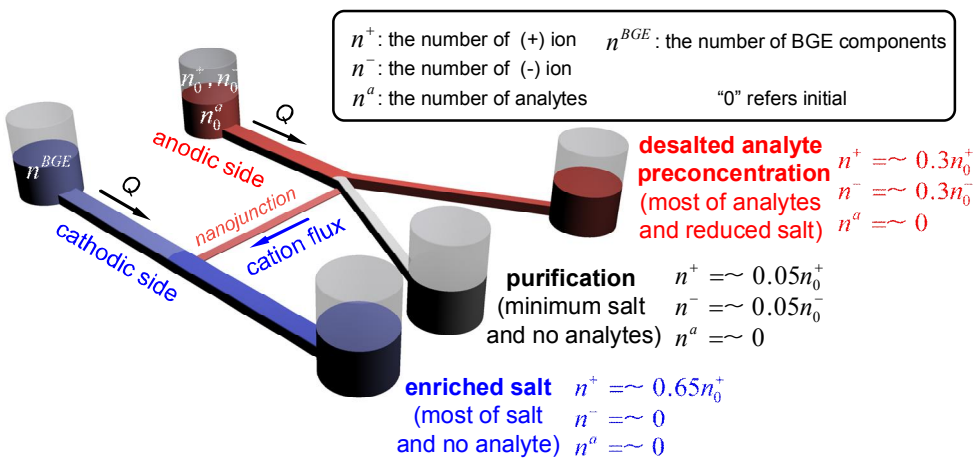

Figure 2.11: The complete mapping of ion and analyte distributions caused by ICP. Each outlet would be utilized as a "desalted analyte preconcentration", a "purification" and an "enriched salt" passage.

Rest of n_0^+ (*i.e.* 65 %) was transported across the nanojunction so to exit through the cathodic side microchannel (blue), and n^- (*i.e.* 65 %) was consumed by electrode reaction to satisfy electro-neutrality condition with

n_0^+. Therefore, we clearly concluded that ICP purification and "desalted analyte preconcentration" mechanism were caused by the consumption of the ions which is a driving source to sustain ICP phenomenon.

2.2.3 Separtion of ions at the inside ion depletion zone

In order to confirm that the concentration difference of Li^+ and Na^+ ions due to ICP, 5-branched micro/nanofluidic device was fabricated as shown in Figure 2.12. The mixture of LiCl (20 mM) and NaCl (20 mM) was pumped across the ion depletion zone and the most of ions were expelled from the zone. While the slip velocity measurement experiments were conducted with 1 mM of samples, 20 mM of samples were used in this experiment because the concentration above 20 mM would guarantee the reliable measurement at the outlet 1 which was the closest outlet from the membrane.

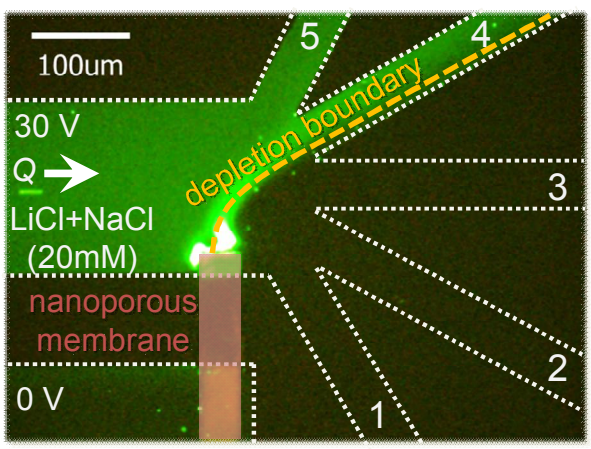

Figure 2.12: Experimental demonstration of ion separation at the inside IDZ by using 5-branched device [33]. The discretized samples from ICP layer was collected in each reservoir.

Since the sample was continuously injected, the deionized samples were constantly collected at each branch so that the concentrations around the ICP layer was able to be discretized. Samples were collected in each outlet reservoirs (from 1 to 5) and measured, and calculated reassigned concentration distribution due to ICP by eq. (7). The results were shown in Figure 2.13. Remarkably, the concentrations of Na^+ were higher than that of Li^+ only at the outlet 1 and 2, while the quantities were inversed at the outlet 3, 4 and 5. Since the induced electric field inside the IDZ was highly amplified up to 100,000 V/m scale [60], hydrated ions in a water solution would be dehydrated [65] as shown in Figure 2.14. Generally, the mobility of the hydrated Li^+ is higher than that of the Na^+, but the mobility of the dehydrated Na^+ is higher than that of the Li^+. Therefore, the inversion of concentration was generated between outside and inside the IDZ. This result would be a strong direct evidence for the field-induced mobility change caused by ICP phenomenon.

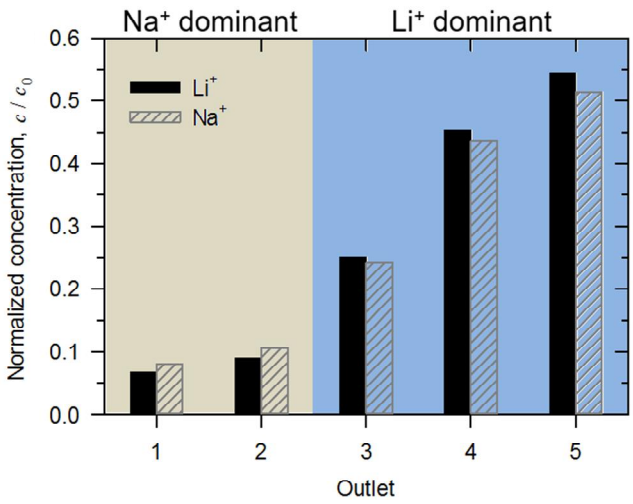

Figure 2.13: A quantitative concentration measurement of each cation [33]. The result showed that the dominance was inversed between outlet 2 and 3.

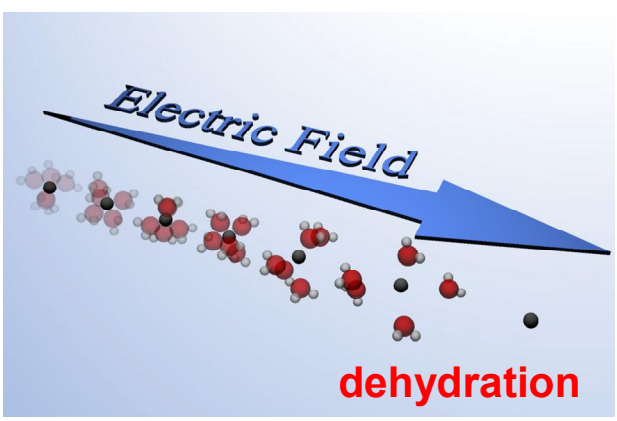

Figure 2.14: Schematic diagram of dehydration of ion in a water solution under strong electric field. Since the induced electric field inside the IDZ was highly amplified up to 100,000 V/m scale [59], hydrated ions in a water solution would be dehydrated.

2.2.4 Concentration modulation of ions at the ion enrichment zone

At the previous Chapter 2.2.2, we confirmed that almost 65 % of cations were transported through the nanojunction from the anodic to the cathodic side of it. Therefore, as shown in Figure 2.15, we proposed a device for collecting cationic species and controlling the concentration enhancement factor by modulating the flow rates at the anodic and the cathodic side microchannel. Mixed electrolyte of Li^+ and Na^+ ions were injected into the anodic side inlet reservoir and the changed concentration values of each cation due to triggering ICP were measured at the cathodic side reservoir.

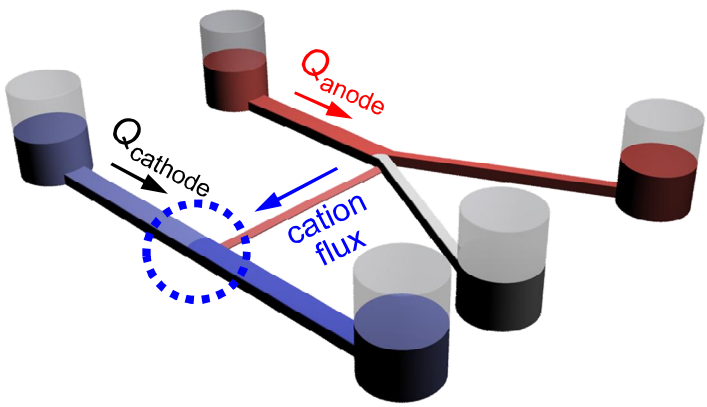

Figure 2.15: Schematic diagram of concentration modulating at the region of IEZ. Concentration enhancement factor at the cathodic side would be modulated by controlling the flow rates at the anodic and the cathodic side of microchannel.

The results were shown in Figure 2.16. The ratio of concentration amplification was slightly over than 1 when the flow rate of the anodic and the cathodic side were the same. However, the ratio of concentration amplification was over than 5 when the flow rate of the cathodic side were 9 times lower than that of the anodic side, Therefore, we concluded that the concentration enhancement factor can be adjusted by modulating a flow rate of each stream at the anodic and the cathodic side. In addition, regardless of the flow rate, the concentration of Na^+ was always higher than that of Li^+ since the electrophoretic mobility of Na^+ in a water solution was 1.3 times higher than Li^+.

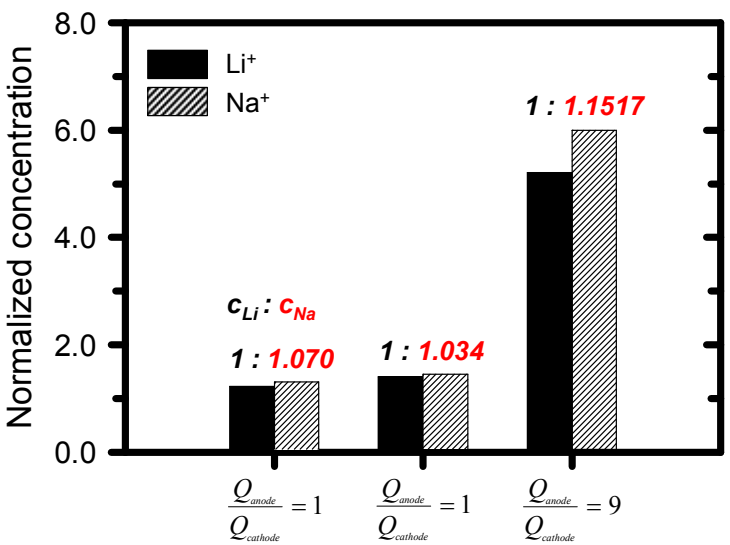

Figure 2.16: The measured and calculated concentration of Li^+ and Na^+ ions. The amplification ratio at the cathodic microchannel can be adjusted by modulating the rate of Q_{anode} and $Q_{cathode}$. Additionally, the concentration of Na^+ was always higher than that of Li^+ regardless of the flow rate.

Chapter 3 Application for ink recycling

3.1 Appropriateness of ICP for recycling ink production

One of the most important process in the chemical industries is a preconcentration and a desalting process that enables to recover only target molecules without the accumulation of unwanted salt for producing high purity chemical particles (or analytes). While evaporation [66] and precipitation [67-70] are major preconcentration techniques in a high capacity plant system, nowadays, nano/bio technologies are gradually growing up to satisfy the need for lab scale small volume of samples such as DNA, proteins and other artificial substances. For these process, high purity and minimum-loss extraction from raw materials becomes critical techniques. Centrifuge [71-73] he only generalized technology in small scale system but its mass based physical separation ability shows obvious limitations such as irregular recovery rate for different samples and significant amount of losses due to repeated steps for obtaining target concentration.

Desalting is also the important technology in the biomedical and chemical industries. Reverse osmosis [74-76] is representative but its utilization is suitable for large scale system due to escalated energy consumption depending the source concentration and additional filtration steps for large molecules. In a lab scale, ultrafiltration [77-79] and desalting

column [80-82] are mainly utilized and show appropriate desalting ability, but high sample losses are entailed, especially, for the substances under ~1 kDa [83].

Generally, the combined technology of preconcentration and desalting are highly demanded for a chemical production. For example, high salinity solution should be added for salt-out process to precipitate target micro/nano particle or protein from prepared sample [84]. At this point, the target particle or protein was precipitated in high salinity environment so that additional desalting processes should be followed. The same process is required for a high quality recycled ink production for inkjet printer. Ink molecules should be concentrated to have a proper viscosity and should be desalted to minimize salt content which causes low printing quality or nozzle blocking. However, more than 2 step processes are necessary to achieve both preconcentration and desalting from a raw material solution. Furthermore, ink recovery rate would be very low if filtration process is applied to desalting because the molecular weight of ink is typically less than ~1kDa.

Figure 3.1 showed that the real image of lab sample (industry graded unrefined ink; acid red 52 with high salt impurity), recycled ink product, 1st filtrated and 2nd filtrated lab sample. It was first tried to desalt using a filtration process to remove the salt from unrefined ink solution. As shown in Table 3.1, salt was successfully removed as expected but the concentration of ink molecule was too lowered to utilize as a commercial

product after the filtration process. Therefore, we concluded that filtration technology was not suitable for the recycled ink production industry.

Figure 3.1: The real image of recycled ink samples. Filtration technology was not suitable for the recycled ink production because it showed very low recovery rate of ink molecules.

Lab sample	Sodium (Na^+)	8310.00	mg/L
Product	Sodium (Na^+)	4413.75	mg/L
1^{st} filtration	Sodium (Na^+)	1587.75	mg/L
2^{nd} filtration	Sodium (Na^+)	39.32	mg/L

Table 3.1: The salinity content of the recycled ink samples. Filtration technology showed high desalting ratio, but it was a higher specification than the recycled ink quality required.

3.2 Desalted ink preconcentration by ICP

Here, for the first time, we proposed a new technology that lossless analyte preconcentration and desalting were simultaneously done in one step called "desalted analyte preconcentration" process. In this work, we exemplified a high quality ink production as the process. Bifurcated microchannel was fabricated to separate infused stream into two streams; one for recovering the fluid with ink molecules (outside the IDZ) and the other for extracting the purified fluid (inside the IDZ). The dimension of both anodic and cathodic side microchannels were 200 um width and 15 um depth. Nafion nanojunction was patterned under bifurcation point of the anodic side microchannel as an exit of salts.

Industry graded unrefined ink was initially injected into the entrance of anodic side microchannel, while transparent sodium chloride electrolyte (380 mM) was injected into the entrance of cathodic side microchannel to balance the ion concentration at the anodic side.

As shown in Figure 3.2, it was visibly observed that ink molecules were repelled from the ion depletion boundary so that most of them were collected at the upper channel (1^{st}), while purified stream was heading toward the lower channel (2^{nd}) with the applied voltage of 100 V at the flow rate of 50 nL/min. Firstly, to verify quantitative concentration variation of ink molecules, color intensity profile was measured across the line from a point A to A'.

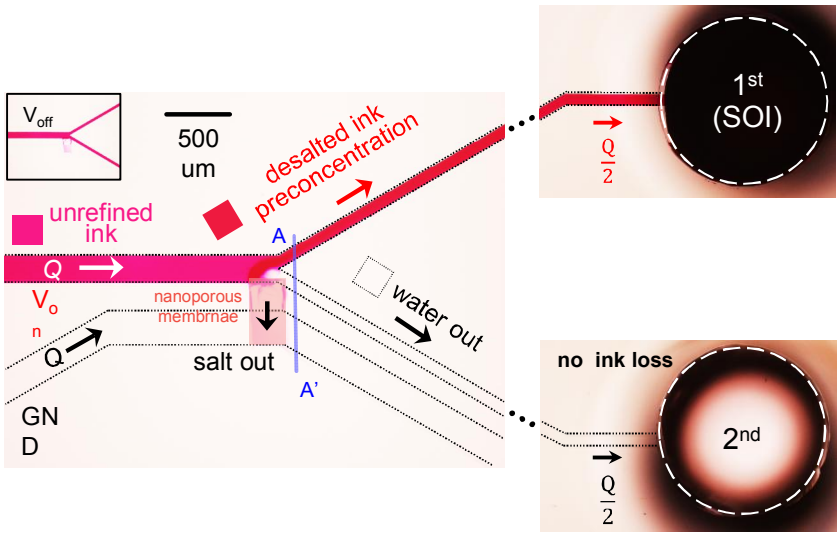

Figure 3.2: The demonstration of the lossless desalted ink preconcentration. After applying an electric field across the nanojunction, ink started to be separated under ion depletion boundaries formation.

As shown in Figure 3.3, ink molecules were equally detected at both upper (1^{st}) and lower (2^{nd}) channel streams before triggering a voltage (t<10 sec, black lines). However, after triggering a voltage (t>10 sec, red lines), the concentration of ink molecules were doubled at the upper channel (1^{st}), while the ink molecules were not detected at the lower channel (2^{nd}) because their color intensity was under the limit of detection regime. Additionally, we confirmed that the ink molecules were undetected at the cathodic side channel (GND) regardless of triggering a voltage. It meant that there was no leakage toward the cathodic side channel (GND) and the lower channel (2^{nd})

so that lossless ink molecule preconcentration at the upper channel (1st) was achieved.

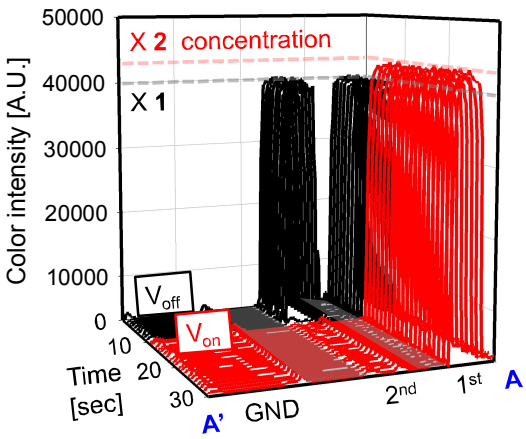

Figure 3.3: Color intensity measurement for the ink molecules concentration. All of ink molecules (Acid Red 52) were collected at the upper channel after triggering a voltage (red lines).

To verify Na^+ transportation in this process, we collected samples from each outlet reservoir of the upper (1st), the lower (2nd), and the cathodic side channel (GND), and measured the concentration values of Na^+ as shown in Figure 3.4.

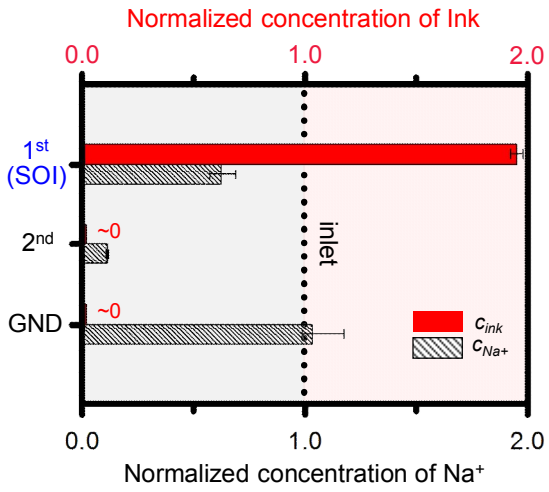

Figure 3.4: Normalized concentration of Na^+ and ink molecules at the upper (1^{st}, SOI), the lower (2^{nd}) and the cathodic side channel (GND). The concurrent process of "desalted analyte preconcentration" was successfully carried at the upper (1^{st}, SOI) channel.

x-axises were normalized by their infused inlet concentration values. In this result, we successfully verified that the upper channel (1^{st}) was desalted (~40 %) with keeping most of ink molecules preconcentrated (~200 %) so that undesirable salt rejection and no-loss of ink molecule preconcentration were simultaneously performed by a single step process, achieving the "desalted analyte preconcentration". In terms of the number of ions, the removal efficiency of salt (Na^+, Cl^-) was calculated ~70 %. Additionally, ~95 % of salt was removed at the lower channel (2^{nd}) to be purified process as the same as previous desalination reports. Note that the remaining Na^+ was mostly transported through the nanojunction and Cl^- was mostly

consumed by electrode reaction to satisfy the mass balance of the whole system.

Chapter 4 Application for artificial kidney

4.1 Artificial kidney based on peritoneal dialysis

4.1.1 Necessity for portable artificial kidney

Although the most expensive medical treatment per patient is chronic kidney disease, the number of chronic kidney disease patients have been increased sharply as shown in Figure 4.1 and Figure 4.2 [85]. The worst thing is that kidney disease cannot be recovered by itself. Transplantation is the only solution to recover kidney function, but it has a risk of immunological rejection. Therefore, in-vitro medical treatments such as hemodialysis (HD) and peritoneal dialysis (PD) are mainly performed to replace kidney function. See Figure 4.3 [85]. The most preferred treatment is HD. The patients should go hospital 3 times a week and stay 8 hours in a day, so it is impossible to keep daily life. PD guarantees daily life unconstrained from hospital, but periodical replacement of dialysate and long exchange time of it are exceedingly inconvenient for patients themselves. PD is a recently introduced treatment which uses peritoneum as a membrane so that dissolved substances such as urea, creatinine (CRN), albumin (ALB), and other toxins in the blood are exchanged with injected pure dialysate (~2 L) by mass transfer. After diffusion and osmotic chemical exchange from blood to dialysate about 2 hours, used dialysate is withdrawn. Then this whole cycle is manually repeated in every 4 to 6 hours in a day

[86]. It is inconvenient and little bit dangerous, for example, 10 L of pure dialysate should be carried for the daily life and patient have a risk of self-replacement. Therefore, patients do not prefer PD. These inconveniences would be resolved by a portable dialysate regeneration system. It should be capable of automatic withdrawing, purifying the used dialysate and refilling the recycled dialysate into peritoneum. Among a number of components, the efficient purification of biological toxic substances would be the key building block. While few mechanisms such as biochemical adsorption or physical filtering has been suggested, the performance was beyond the criterions.

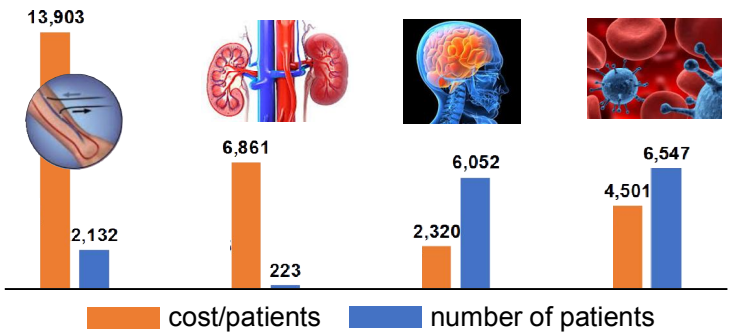

Figure 4.1: The diagram of cost per patient and the number of patients for the disease [85]. The most expensive medical treatment per patient is chronic kidney disease.

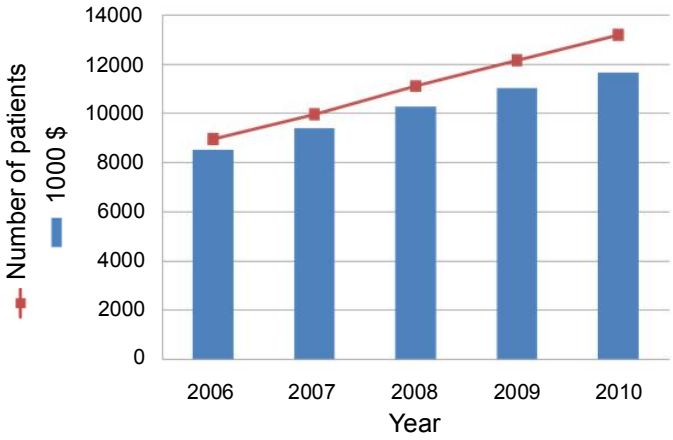

Figure 4.2: The diagram of the number of patients per year and the total cost for the chronic kidney disease patients [85]. The number of chronic kidney disease patients have been increased sharply.

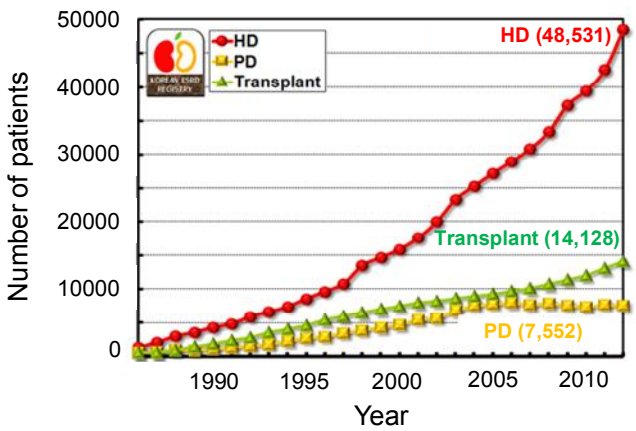

Figure 4.3: The diagram of the number of chronic kidney patients per year for the hemodialysis (HD), peritoneal dialysis (PD), and Transplant [85]. Most of chronic kidney disease patients were treated by HD, but patients are hard to maintain their normal life.

4.1.2 Concept for continuous dialysate ICP purifier

Here we proposed the nanoelectrokinetic ICP purifier for the continuous dialysate recycling system as shown in Figure 4.4. Micro wastes in a used dialysate rejected outside ion depletion zone since most of them had an electrical charge and cationic species in a used dialysate was removed by cationic flux through nanojunction. Therefore, we would continuously obtain a purified dialysate by extracting stream from ion depletion zone. Micro/nanofluidic platform was initially investigated to meet the criterions and a 3D printed macro system for practical throughput was also presented.

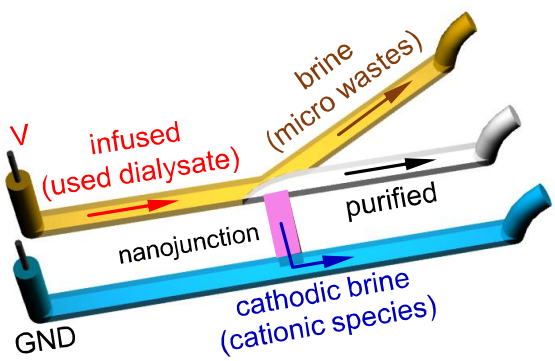

Figure 4.4: Schematic diagram of nanoelectrokinetic purifier for continuous peritoneal dialysate recycler [87]. Micro wastes in used dialysate rejected outside the ion depletion zone since most of them had an electrical charge, and cationic species were transported (or removed) through the nanojunction. Purified dialysate would be obtained from continuous extraction of stream inside ion depletion zone.

4.2 Dialysate purification mechanism by ICP

4.2.1 Demonstration of used dialysate purification

We developed 2-branched bifurcated microchannel device to separate brine, purified, and cathodic brine streams. An external voltage (50 V) was applied across the Nafion nanojunction and both the analyte and the buffer solution (used dialysate, from Seoul National University Hospital) were continuously injected with a constant flow rate (0.1 uL/min) into both the anodic and cathodic microchannels. Under these experimental conditions, we successfully generated ICP phenomenon and developed ion depletion boundary in used dialysate solution as shown in Figure 4.5.

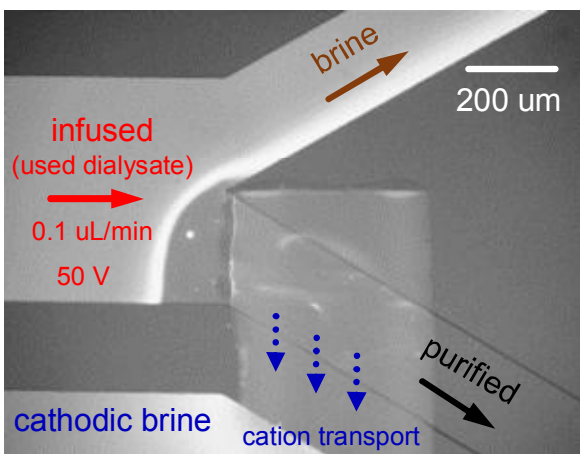

Figure 4.5: Demonstration of ICP purifier [87]. ICP phenomenon was fully developed in a used dialysate solution and formed 3 different streams with applied voltage (50 V) and flow rate (0.1 uL/min) external conditions.

Brine, purified streams in the anodic side and cathodic brine stream in the cathodic side were visibly observed due to ICP development.

As shown in Figure 4.6, we confirmed that ion depletion boundary was stably maintained with external condition of constant bias (50 V) and flow rate (0.1 uL/min) during 180 min. Precipitation near ion depletion boundary was additionally observed over time.

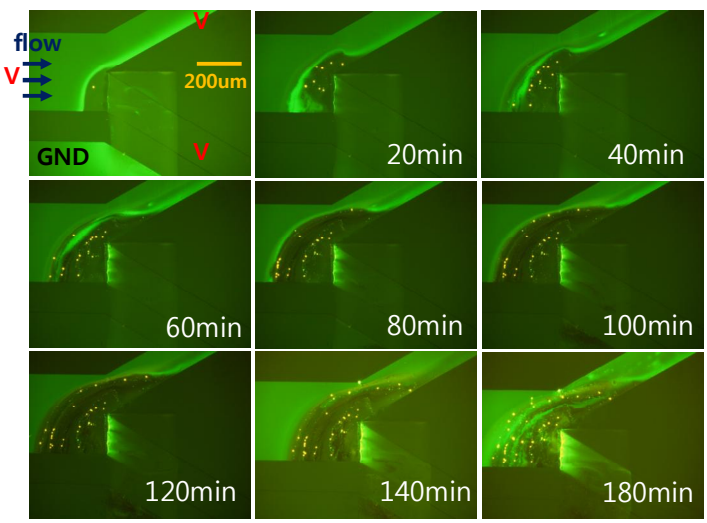

Figure 4.6: Demonstration of operation stability for the ICP purifier. Ion depletion boundary was stably maintained during 180 min.

Each stream was extracted individually and concentration profiles of Na^+, CRN, ALB, phosphorus (P), Cl^-, and urea were quantitatively measured by Renal Panel (HITACHI 7180) as shown in Figure 4.7. The positively charged species (Na^+, CRN) were removed depending on their

electrophoretic mobility. Since Na^+ ion has the highest electrophoretic mobility among major components in used dialysate solution, most (~80 %) of Na^+ ions were transported through the nanojunction by cationic flux and only ~15 % were repelled from ion depletion boundaries so being ~5 % of Na^+ ions were left at the inside ion depletion zone. Finally around 90 % desalted stream was collected. This result was similar to the previous results of Chapter 2. CRN, sub nanometer molecule and one of the major toxin of body wastes from used dialysate, is electrically neutral at pH 7.4 but a positively charged under pH 7.4. Since dialysate showed slightly acidic property, we confirmed that CRN particles showed cation like transportation mechanism under the ICP operation. ~55 % of CRN passed through the nanojunction and ~30 % of them flew through the brine stream. Finally ~15 % of CRN were left at the inside ion depletion zone so that concentration of CRN was decreased around 70 % in the purified stream. It was meaningful that removal ratio of CRN was less than that of Na^+ since molecular weight of CRN (66) was bigger than that of Na^+ (23). ALB is a kind of protein existed in a human body which has molecular weight around 66,000. The result showed that ALB was not pass through the nanojunction by ICP phenomenon but some of it was repelled by ion depletion boundary. Therefore, final concentration of ALB was decreased around 60 % in the purified stream. The removal ratio of ALB was lower than Na^+ and CRN since molecular weight of it was much bigger than them.

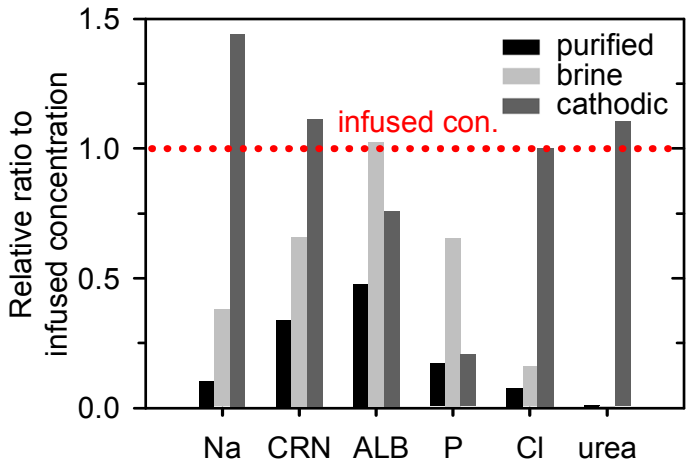

Figure 4.7: Measured concentrations of dialysate components from extracted each stream [87]. The removal ratio of Na^+ was the highest among positively charged substances (Na^+, CRN, ALB) since electrophoretic mobility of it was the highest. ~80 % of Na^+ passed through the nanoporous membrane by cationic flux and only ~15 % of it went through the brine stream. CRN was removed likewise cation removal mechanism but the removal ratio was less than Na^+. ALB showed less removal ratio than Na^+ and CRN. Weakly charged P was mostly precipitated inside a channel and negatively charged Cl^- was consumed by electrode reaction. Neutrally charged urea was completely decomposed in both the purified and the brine stream.

On the other hand, concentration of P was highly reduced at all of the region. Therefore, we collected all of the precipitates from the surface of the microchannel, and investigated the components. See Figure 4.8. Content

increase factor was calculated by dividing dissolved precipitation concentration to used dialysate concentration. It was proven that P was disappeared since most of them was precipitated. From this result, we concluded that weakly charged P could not pass through the nanoporous membrane and precipitated on a channel surface.

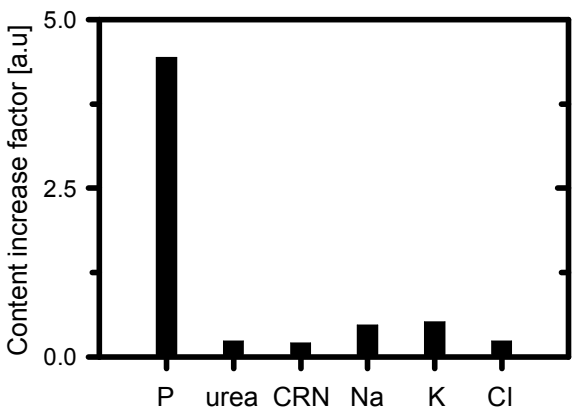

Figure 4.8: Diagram of content increase factor calculated by dividing dissolved precipitation concentration to used dialysate concentration. The concentration of P was the most because weakly charged P could not pass through the nanoporous membrane and precipitated on a channel surface.

Negatively charged Cl^- was consumed by electrochemical reactions on the anodic electrode so to satisfy electro-neutrality in a solution due to ICP which rearranged concentration profiles near nanojunction. Remarkably, urea (known as uncharged molecule), one of the major toxin of body waste

along with CRN, was completely eliminated both at the brine and the purified streams. Following section would explain cause of elimination.

4.2.2 Removal mechanism of body toxins (urea, creatinine)

To confirm removal mechanism of urea and creatinine in used dialysate solution, control experiments were done with various types of junction and electrode. Firstly, non-ICP condition was demonstrated without using nanojunction in a microchip as shown in Figure 4.9. Electrodes were set inside a single microchannel without any junction and filled in used dialysate solution. Positive voltage and pressure were applied in anodic reservoir, and outward stream was collected from cathodic reservoir. In this case, only urea was completely eliminated and other species were remained without any change. We obtained same results when microjunction was built between anodic bifurcated microchannel and cathodic microchannel instead of building nanojunction.

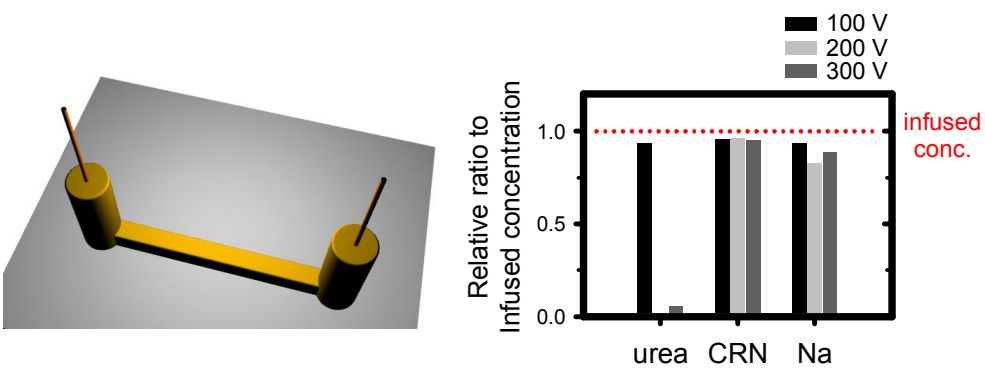

Figure 4.9: Control experiment of non-ICP condition to verify toxins removal mechanism. Only urea was completely eliminated and other species were remained without any change.

It was reported that urea was decomposed to nitrogen and carbon dioxide gas at high potentials (over 1.7 V versus SCE) by direct oxidation process at the electrode surface as following equations [88-91]. Eq. (10) refers anodic reaction, eq. (11) refers cathodic reaction, and eq. (12) refers the overall reaction.

$$CO(NH_2) + 6OH^- \rightarrow N_2 + 5H_2O + CO_2 + 6e^- \quad (10)$$

$$6H_2O + 6e^- \rightarrow 3H_2 + 6OH^- \quad (11)$$

$$CO(NH_2) + H_2O \rightarrow N_2 + 3H_2O + CO_2 \quad (12)$$

While at lower potentials (below 1.6 V versus SCE) or natural oxidation condition, urea decomposed to nitrogen oxidation components which is harmful to human body [90, 91], nitrogen and carbon dioxide gas product from ICP decomposition are harmless to the human body.

Secondly, ICP condition was implemented with using nanojunction in a microchip. As we mentioned in the previous section, urea was completely eliminated and other species were removed by electrical transportation due to ICP phenomenon. To separate ICP and electrochemical removal mechanism, we built 3 independent microchannels, one for anodic at the top side, another for sample flowing at the middle side and the other for cathodic at the bottom side as shown in Figure 4.10. In this case, ICP was still successfully developed at the middle bifurcated channel by electric field

across the nanojunction from top anodic channel to bottom cathodic channel. Urea was remained without any change, but creatinine and Na^+ were removed by electrical transportation due to ICP phenomenon.

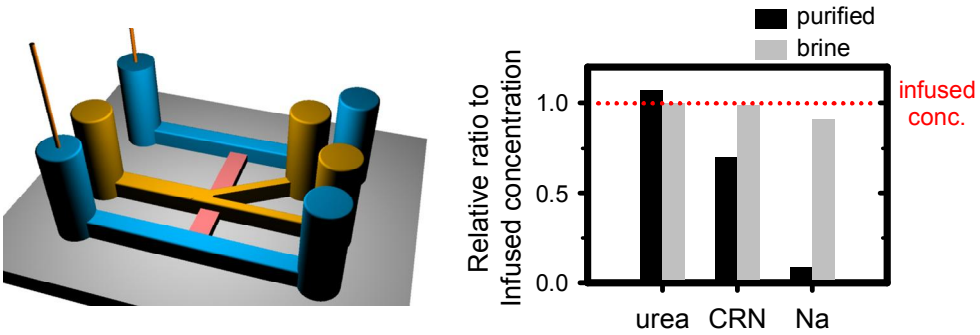

Figure 4.10: Control experiment of ICP condition separated with electrochemical reaction. Urea was remained without any change, but creatinine and Na^+ were removed by electrical transportation due to ICP phenomenon.

4.2.3 The pH measurement

We measured the pH of the dialysate solution purified by ICP phenomenon as shown in Figure 4.11. The pH of the used peritoneal dialysate was about 7.7, which was close to neutrality. In the case of only microjunction without nanojunction, the pH was almost the same as initial value at both the anodic and cathodic sides due to only the electrochemical reaction. On the other hand, in the case of nanojunction, the ICP phenomenon was developed, and the selective cation transportation to the cathodic side of the nanojunction was activated, and the pH was decreased to 5. This pH value is similar to the distilled water level. In Chapter 2.2.2, we showed that the negative ions were dissipated from the electrode as an electrochemical reaction in order to satisfy the neutral conditions of the positive and negative ions at the anodic side as the positive ions were transported through the nanojunction. However, in the used peritoneal dialysate solution, a variety of electrochemical reactions including urea decomposition reaction were proceed, so that the removal rate of anions was relatively decreased. Therefore, as the hydrogen ion was generated, the pH was decreased while adjusting the electrical neutrality balance between the cation and the anion. At this time, hydrogen ions were generated as final products of urea decomposition and water decomposition reaction. On the other hand, at the cathodic side, a large amount of cations were transported through the nanojunction, and OH- ions were created by the water decomposition

reaction, thereby satisfying the electrical neutral condition and increasing the pH.

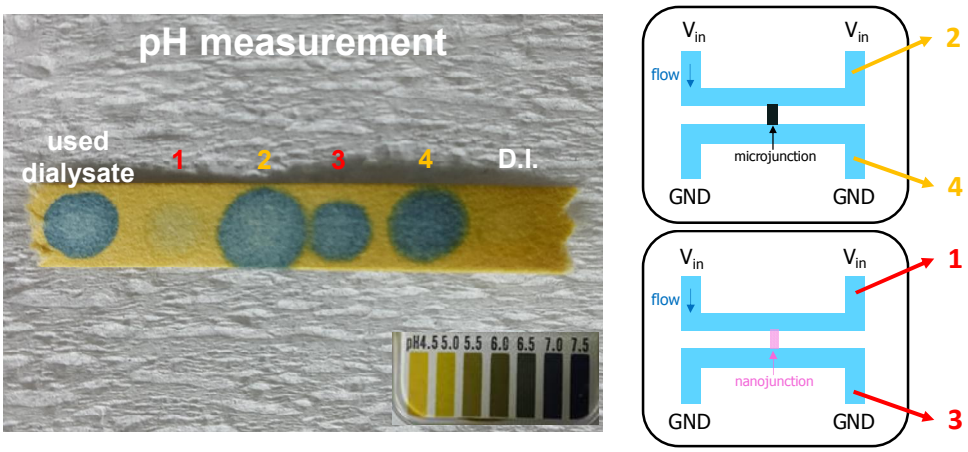

Figure 3.11: The *pH measurement of used dialysate purification without and with nanojunction. While the pH was almost the same as initial value at both the anodic and cathodic sides in the case without nanojunction, decreased to the level of distilled water in the case with nanojunction.*

In fact, the pH of the new peritoneal dialysis solution was injected into the abdominal cavity at about 5, and the pH was increased to about 7.7 by the substance exchange in the peritoneal membrane and was discharged to the outside of the body. Therefore, the dialysate purified at pH 5 level was expected to be harmless to the human body since it was at a pH level similar to that of the new dialysate.

4.2.4 Appropriateness of ICP technology for artificial kidney

From these results, we found out two key conclusions. First, urea was eliminated not by ICP phenomenon but by electrochemical decomposition. Since urea was electrically neutral molecule, it did not change its traveling direction with or without ion depletion boundary layer. It was observed that urea was participated in electrochemical reaction on the electrode surface. Second, the successful dialysate purification would be achieved only when ICP was triggered by a directly contacted electrode with infused stream. Specific conditions for a dialysate purification was shown in Table 4.1.

	Junction Type	Electrode type	Schematic	Relative ratio of purified to infused (%)					
				Na	CRN	ALB	P	Cl	urea
non-ICP	x	direct	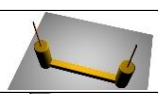	100	100	100	100	100	0
	micro	direct	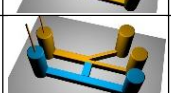	100	100	100	100	100	0
ICP	nano	direct	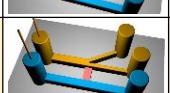	10	30	45	15	5	0
	nano	indirect	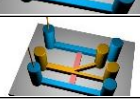	10	30	45	15	100	100

Table 4.1: Control experiments results for the specific dialysate purification condition [87]. Na^+, CRN and ALB were removed during ICP operation while urea was decomposed only with directly contacted electrode to the infused stream, regardless of ICP operation. Urea was unaffected by the ion depletion boundary layer, and participated in electrochemical reactions on the electrode surface.

4.3 Throughput enhancement by using fin structures

4.3.1 Fin installed continuous ICP separator

The fin structures were applicable for a continuous type ICP separator. The continuous type ICP separator was utilized in electro-desalinator [51] and continuous biomolecular preconcentrator [43] as well. While the preconcentration factor was limited by the dimensional ratio of bifurcated microchannels, the sample in a purified stream largely desalted over 100 times in both applications so that ICP separator was more useful for the desalination or purification applications than the preconcentration applications. The combination of external flow which was capable of bursting the ion depletion zone would be the key mechanism of ICP separator [51, 60]. Any charged species flown through the main microchannel was vertically (upwardly) repelled from the nanoporous membrane so that their path would be deflected toward the upper brine microchannel. In these operations, high-throughput sample collection would be essential for further practical development. A fin installed ICP separator was shown in Figure 4.12. The main microchannel (red) had the dimension of 5 mm width and 15 um depth before the bifurcated point. By the serially-varied length of fin structures, the brine and the purified channel was designed to have the same fluidic resistance based on numerical simulation results. Consequently, an interval between each fin was set to be 100 um and lengths of them were gradually increased from a bottom-most fin to a

top-most fin to regulate the pressure field. The nanoporous membrane was slantly patterned to assist the upward migration of charged species.

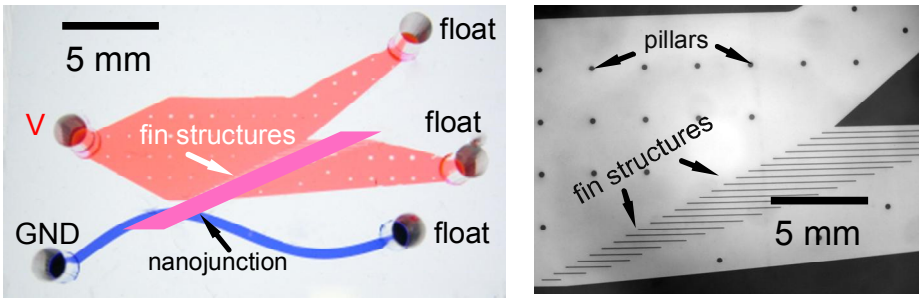

Figure 4.12: A microscopic image of high-throughput continuous ICP separator and magnified image near the fin structure [92]. Pillar array was installed to prevent the collapsing PDMS.

The sample (KCl 1 mM) was continuously injected from the inlet of main microchannel (Q = 4 uL/min) with an electrical voltage (110 V). Two outlet reservoirs were floated and the buffer microchannel was grounded. Figure 4.13 showed that unstably formed fluctuating plugs along the nanojunction in a millimeter scale macrochannel without fin structures. This was because multiple random vortexes vigorously fluctuated back and forth, leading to dispersed preconcentration stream and leakages which should result in low purification or preconcentration ratio. Compared to this unstable operation, however, the fin assisted macrochannel had a quiescent ICP operation which resulted in narrowly defined preconcentration stream as shown in Figure 4.14, confirming the important role of fin structure. 3-

dimensional plots in Figure 4.13 and Figure 4.14 would verify the progression of the filtration or preconcentration process.

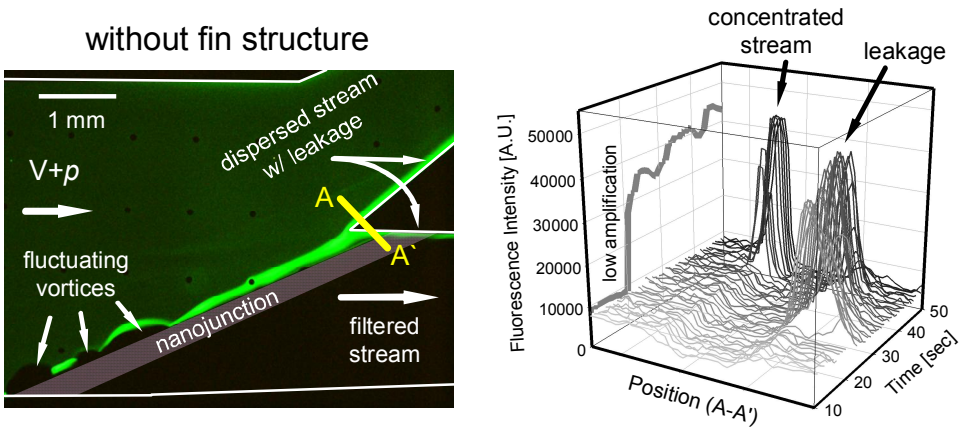

Figure 4.13: The microscopic snapshot of the filtration process without the micro fin structures and their fluorescent intensity plot [92]. Dispersed stream with leakage through the nanojunction was visibly observed.

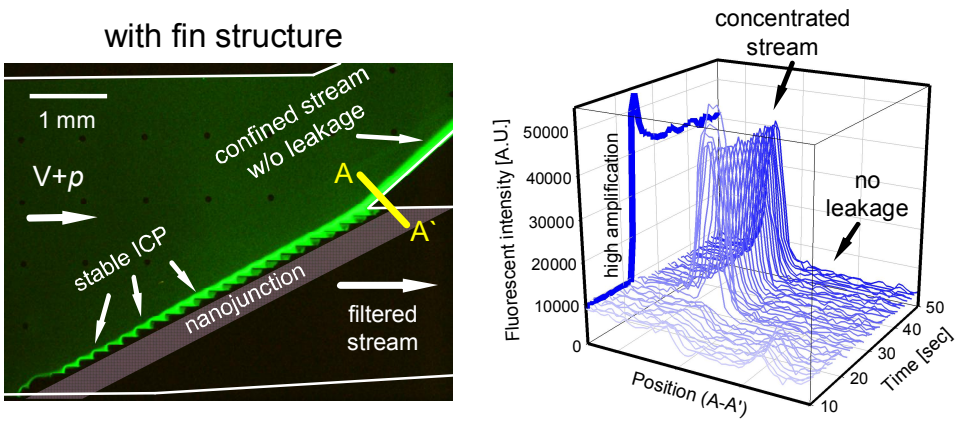

Figure 4.14: The microscopic snapshot of the filtration process with the micro fin structures and their fluorescent intensity plot [92]. The fin structure was able to achieve higher preconcentration enhancement and less fluctuation.

Fluorescence intensity of preconcentrated stream was measured in time-revolving manner to confirm that the fin structure assisted to efficient filtration (or rapid preconcentration) and stabilization of the stream, *i.e.* shaper increase and no fluctuation with the fin structure by comparing grey and blue solid line. The values of maximum fluorescent intensity at each time-span were choose to plot the lines in *x*-*z* plane.

4.3.2 Fabrication of macro-fluidic device using 3D printer

To extend these findings in micro and nanofluidics toward a practical dialysate recycling application, 3000 times throughput enhanced macro-fluidic device was fabricated with a 3D printer as shown in Figure 4.15.

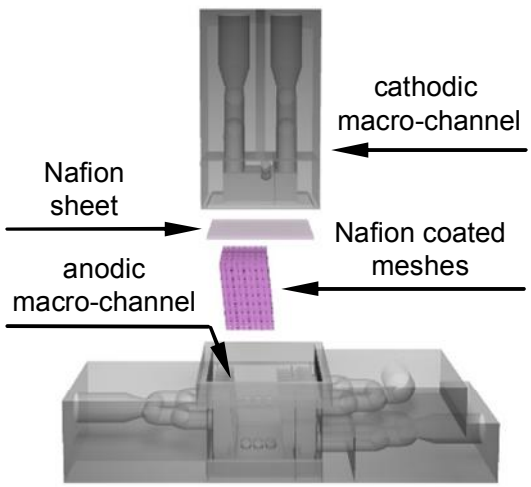

Figure 4.15: Exploded view of 3D printing blocks for a macro-fluidic device [87]. To assemble a macro-fluidic device, nanoporous Nafion sheet and Nafion coated mesh blocks were inserted between anodic and cathodic macro-blocks.

The expansion of ICP layer is requisite to filter dialysate at macrofluidic system. Thus, we contrive the novel system which has Nafion coated mesh as a key structure. The frame of the mesh is made of 3D-printed photopolymer and coated by Nafion. It performs as the transportation pathway of cations to arise ICP, which carries out the similar

role of surface-patterned Nafion at micro/nanofluidic system. The mesh was designed to maximize contacting area with dialysate flux, for high cation transportation rate. Divided by Nafion sheet, cations migrates from anodic macro-channel to cathodic macro-channel without flow interference. Cations are depleted at the vicinity of Nafion sheet after applying electric field from anodic to cathodic channel. The mesh performs as the medium to expand ion depletion layer, which enable to occur only thin (<100 um) depletion layer if there were no mesh structure. Anodic electrode is located on brine channel and cathodic electrode is located on buffer channel. The products from electrode reaction go to each brine and buffer channel so that do not affect to purified dialysate. Assembled macro-fluidic device was shown in Figure 4.16.

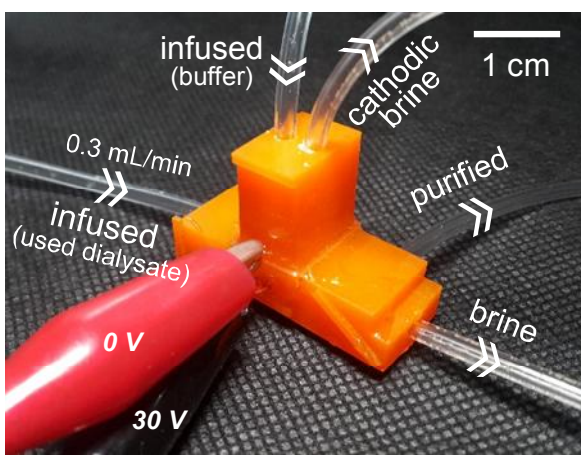

Figure 4.16: The assembled macro-fluidic device [87]. 0.3 mL/min and 30 V external sources were applied to the device and the purified, the brine and the cathodic brine streams were collected and analyzed.

In order to confirm whether the ICP is well developed inside the fabricated device, the experiment was performed as shown in Figure 4.17 (Nafion coated mesh) and Figure 4.18 (Nafion uncoated mesh). The impedance was increased maximum 40 % in the purified chamber with applying voltage, the brine chamber was slightly increased, and the cathodic side chamber was greatly decreased as shown in Figure 4.17. That is, ion concentration was decreased by up to 40 % in the purified chamber, and the ion concentration was increased in the cathodic side chamber because the rejected ions in the anodic side were transported to the cathodic side of the Nafion sheet. In addition, when the flow rate was reduced from 0.5 mL/min to 0.3 mL/min, the ion exchange process by ICP became more active. On the other hand, Figure 4.18 showed that the concentration change was insignificant even under the same voltage and flow rate conditions as shown in Figure 4.17. This was because the ion exchange process occurred only near the Nafion sheet. Therefore, we would conclude that the Nafion coated mesh played a key role in the generation of ICP by ensuring sufficient ion migration paths in the macro device.

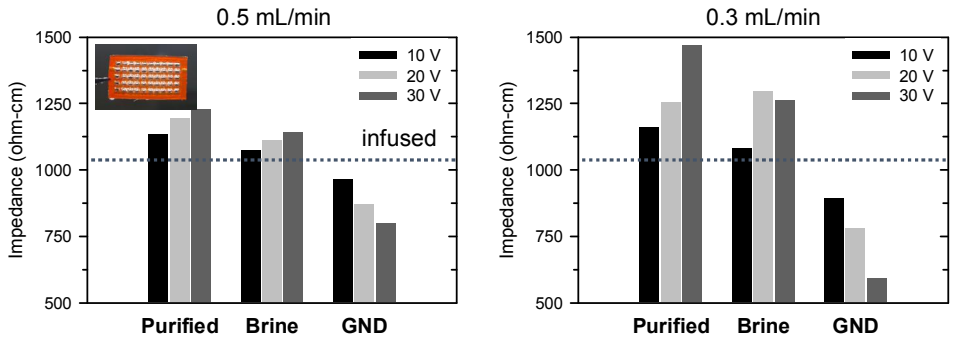

Figure 4.17: Purification performance of assembled microfluidic device with Nafion coated mesh. The impedance was increased maximum 40 % in the purified chamber with applying voltage, and the cathodic side chamber was greatly decreased

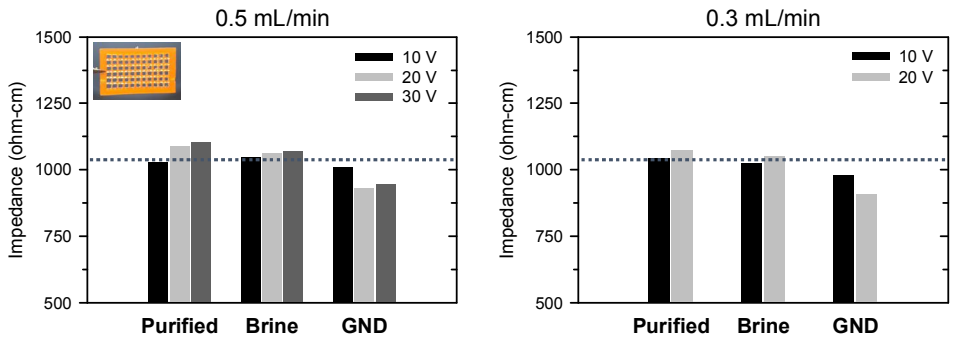

Figure 4.18: Purification performance of assembled microfluidic device without Nafion coated mesh. The concentration change was insignificant even under the same voltage and flow rate conditions as Figure 4.17. This was because the ion exchange process occurred only near the Nafion sheet.

4.3.3 Performance of dialysate purification by macro-fluidic device

The performance of the device depends on voltage and flow rate. Purification ratio enhances as higher voltage at the same flow rate, because more cation transported through Nafion coated mesh. In addition, the products from electrode reaction could bring imbalance of pressure distribution, so that we also consider it to decide voltage and flow rate. At the 0.3 mL/min and 30 V condition, CRN was removed ~30 % and urea was removed over 90 % as shown in Figure 4.19. These removal ratio is enough to running the continuous peritoneal dialysate recycler for several physiological reasons, while the condition for potable water is much restricted. Throughput could be increased by stacking the devices with identical operation principle.

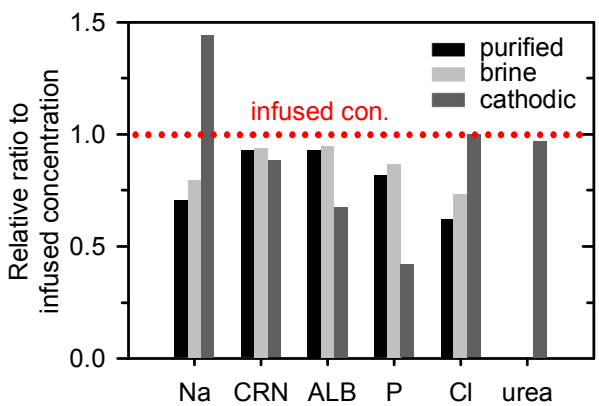

Figure 4.19: Removal efficiency of the macro ICP purifier [87]. The results satisfied the operation criteria of the continuous dialysate recycler (~30 % removal) with completely removed urea.

4.4 Macro device for practical utility

4.4.1 The 10 mL/min capacity throughput macro device

Figure 4.20 shows the evolution of water treatment capacity to develop a target capacity of 10 mL/min that can be adapted as an artificial kidney.

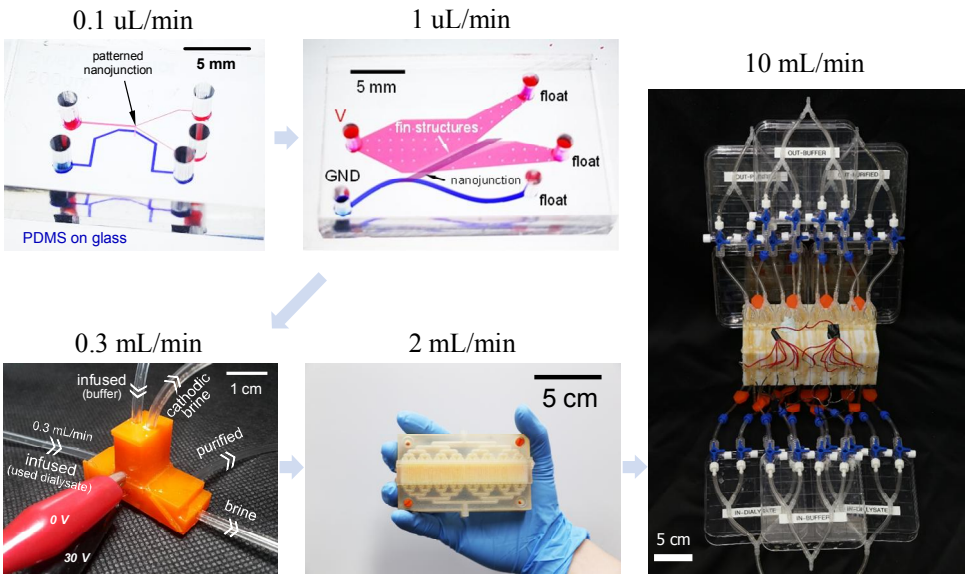

Figure 4.20: The evolution of water treatment capacity to develop a target capacity of 10 mL/min that can be adapted as an artificial kidney. Throughput was increased from 0.1 uL/min to 1 uL/min by using the 2D fin structures at the micro-nanofluidic platform, and 0.3 mL/min by using the 3D fin structures coated with ion exchange resin at the macrofluidic platform. 100,000 times increased 10 mL/min was developed by parallelization of 0.3 mL/min device.

We increased the throughput from 0.1 uL/min to 1 uL / min by using the 2D fin structures at the micro-nanofluidic platform, and succeeded to develop 0.3 mL/min by using the 3D fin structures coated with ion exchange resin at the macrofluidic platform. However, in order to produce the actual artificial kidney, it is advantageous to continuously remove only the body toxins such as urea and creatinine and some ions, and to preserve the other protein components. Therefore, it was better to make device operate long time by eliminating the volume loss due to the dialysate flowing through the brine chamber which contained a small amount of creatinine and a large amount of protein rejected by the ion depletion boundary. As refer to the microfluidic results shown in Table 4.2, we made a strategy to design a single channel by combining the brine and the purified chamber at the anodic side. Large amount of creatinine would be removed through only the nanoporous membrane and most of urea would be removed by the electrochemical reaction at the anodic side same as previous results.

A single module device with a throughput capacity of 2 mL/min was fabricated from a unit cell of the modulated 0.3 mL/min throughput device which had one single purified chamber without the brine chamber at the anodic side. And eight single modules were connected in parallel to finalize a multiple module device having a processing capacity of 10 mL/min. In the final, we successfully developed a macro ICP purifier which was increased throughput of 100,000 times compared with micro-nanofluidic device

		2 way separation (brine, purified)	**1 way** separation (purified)
schematics		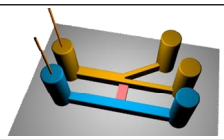	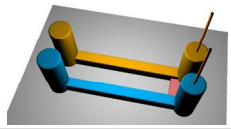
visible results		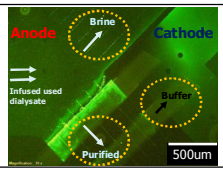	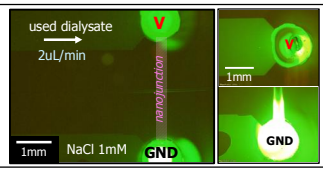
purified / reference [%]	**urea**	**0**	**15**
	CRN	**20**	**30**
	Na	10	50
	uALB	45	60

Table 4.2: Removal efficiency of the macro ICP purifier. The results satisfied the operation criteria of the continuous dialysate recycler (~30 % removal) with completely removed urea.

4.4.2 The electrode for biocompatibility

When the voltage was applied to Ag electrodes emerged at the device in which the used dialysate was injected, the black precipitate generated from the electrode was output at the outlet of the ICP module, or accumulation in the nanoporous membrane or surface of the channel was detected as shown in Figure 4.21. It was predicted that this precipitate was mainly composed of the electrode component dissolved by the electrode reaction and the carbonized dialysate solution. This was because the Ag electrode had a low standard electrode potential of 0.8V or less, which was highly reactive with electrolyte ions in the dialysate solution and formed a large amount of impurities. Therefore, the Ag electrode was replaced with a Pt electrode which had a standard electrode potential of at least 1.2 V. In this case, it was confirmed that the non-biocompatible black carbide was no longer produced as shown in Figure 4.22.

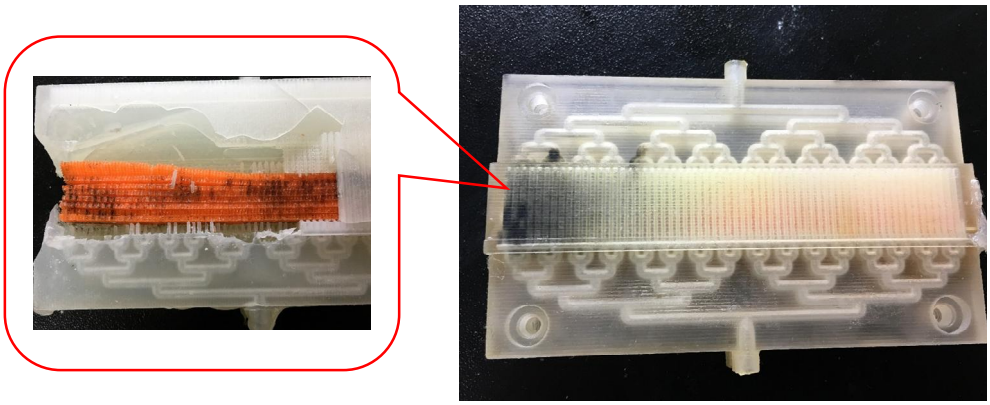

Figure 4.21: Image of the unknown black precipitate generation after dialysate purification process with Ag electrodes. The Ag had a low standard electrode potential of 0.8V or less so that it was highly reactive with components in the dialysate solution.

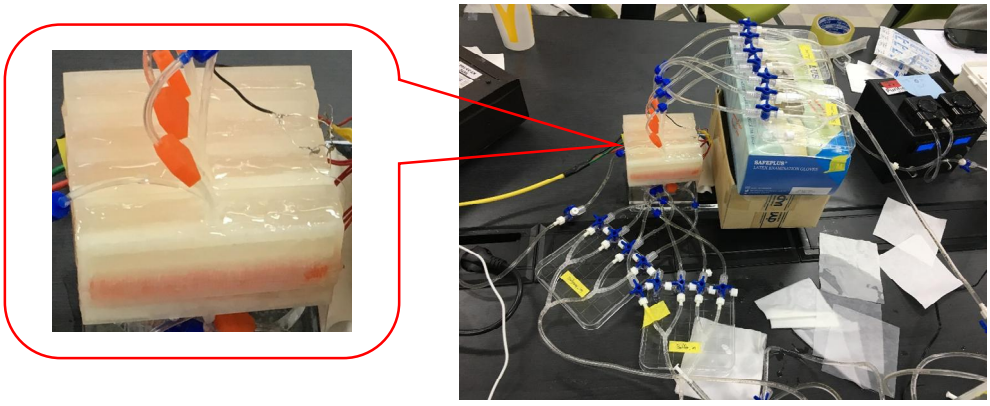

Figure 4.22: Image of the device after dialysate purification process with Pt electrodes. The Pt had a standard electrode potential of at least 1.2 V so that non-biocompatible black carbide was not produced.

4.4.3 In-vitro test

A closed loop experiment was conducted to simulate the circulation of human kidney physiology as shown in Figure 4.23.

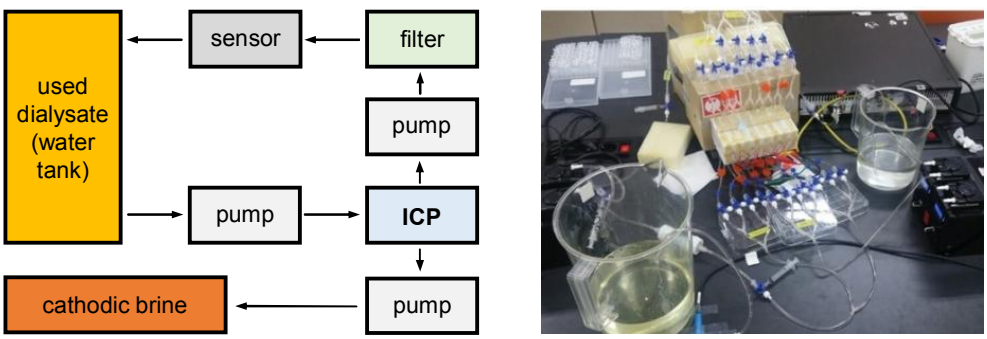

Figure 4.23: The block diagram of closed loop in-vitro test and experimental set-up to simulate the circulation of human kidney physiology. Prepared used dialysate in a water tank, a mimic of abdominal cavity of the human body, was withdrawn by 10 mL/min flow rate and passed through the ICP device, silk fibroin filter and sensor units.

2L of the prepared used dialysate was put into the water tank which is a mimic of abdominal cavity of the human body. The used dialysate in the water tank is first passed through an ICP device at a flow rate of 10 mL/min by the input pump and then passed through a silk fibroin based filter which had strong selective adsorption to creatinine. The purified dialysate was passed through the sensor unit which can monitor the concentration of the

urea and the electrolyte after passing through the output pump for stable maintenance of the flow rate, and discharged again into the water tank containing the used dialysate. The buffer unit corresponding to the cathodic side is implemented so as to have an independent circuit to be circulated. Sampling for the concentration measurement was performed every 20 minutes for an experiment time of 120 minutes.

The results of toxin and ion removal performance evaluation by ICP device alone are shown in Figure 4.24.

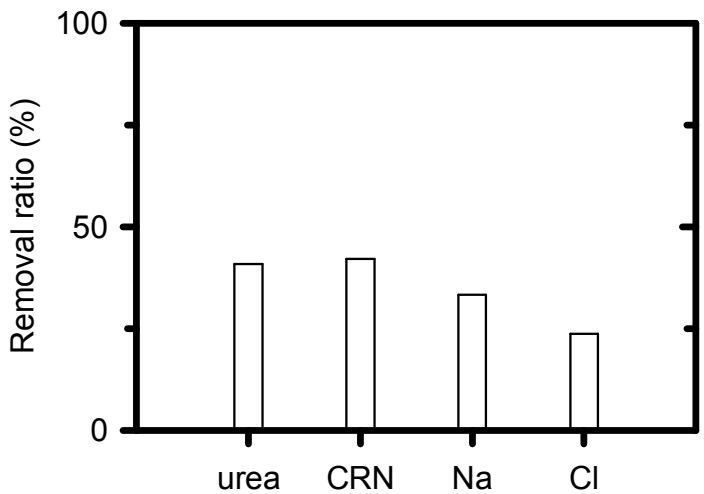

Figure 4.24: The diagram of toxin and ion removal performance by ICP device. The urea was removed ~40 %, CRN was ~40 %, Na^+ was ~33 % and Cl^- was ~25 % after 1 cycle operation.

The urea removal ratio was measured at 40 % level, but it should be more than 90 % removal ratio based on the previous results. This discordance of the removal rate was due to be an instability of the flow rate and electric field distributions in the device. The removal ratio of creatinine was measured at 40 % level, similar to the previous results, but that of Na^+ slightly lowered to 33 %. The concentration of Cl^- was lowered because the electrical neutralization condition must be satisfied in the dialysis solution.

Next, the concentration change of the used dialysate in the water tank, mimic of the peritoneal fluid in abdominal cavity, was measured as shown in Figure 4.25.

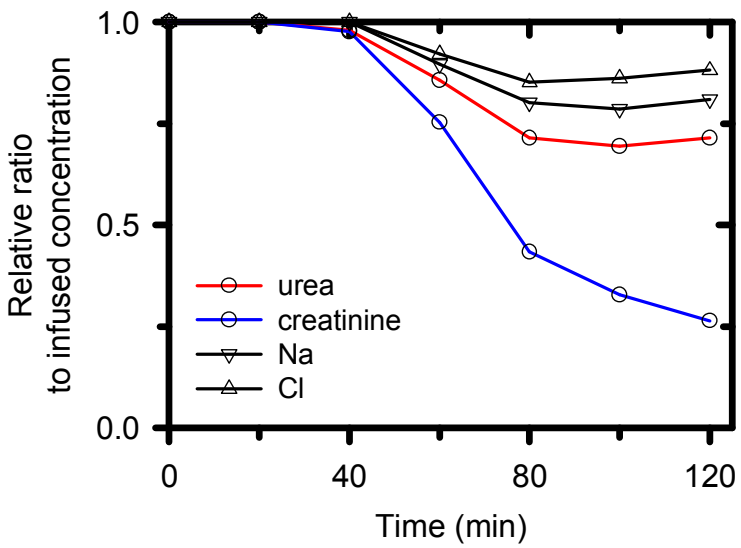

Figure 4.25: The concentration change of the used dialysate in the water tank, mimic of the peritoneal fluid in abdominal cavity. This diagram showed the purified process over time.

The concentration change was not observed until 20 minutes after the initiation of the experiment, but it was steeply decreased after 40 minutes. The concentration of creatinine was maintained at 25% level and the urea level was maintained less than 75 % after 2 hours so that toxin removal was performed well. It can be seen that the concentrations of positive and negative ions are not significantly decreased but slightly decreased within 25 % of the concentration of injected used dialysate.

4.4.4 In-vivo test

The in vivo test was conducted as shown in Figure 4.26 based on the analysis of the removal rate of toxins and electrolytes measured on the closed loop in vitro test performed before. A model of chronic renal failure beagle dog was prepared for the in vivo test, and a peritoneal dialysis environment was created by catheter insertion at the entrance of the abdominal cavity.

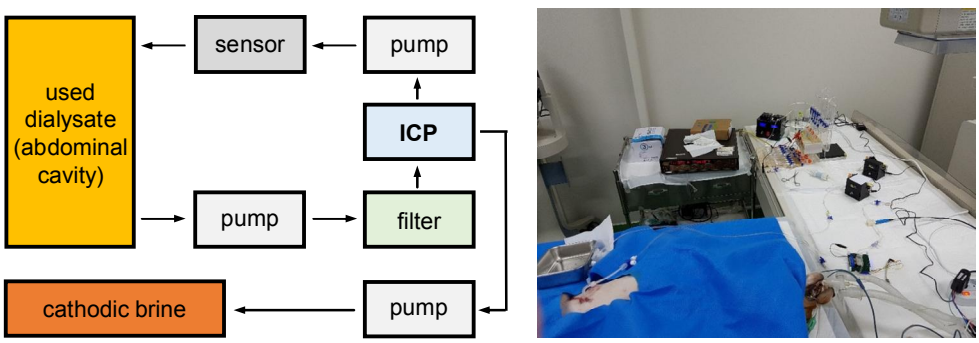

Figure 4.26: The block diagram of in-vivo test and experimental set-up. A model of chronic renal failure beagle dog was prepared, and a peritoneal dialysis environment was created. Firstly pure dialysate was injected abdominal cavity of the dog, and after 4 hours secondly, used dialysate was withdrawn by 10 mL/min flow rate and passed through the ICP device, silk fibroin filter and sensor units, and reinjected into the abdominal cavity of the dog.

2L of new dialysate solution was filled into the abdominal cavity of the beagle dog. After 4 hours, the used dialysate flowing from the abdominal cavity was passed through the silk fibroin based filter and the ICP device to purify. The peritoneal dialysate in the peritoneal cavity was extracted at a flow rate of 10 mL/min by the pump, passed through a filter and ICP device, and then injected into the abdominal cavity again after passing the sensor part for monitoring the concentration of urea and electrolyte. The buffer unit corresponding to the cathodic side is implemented so as to have an independent circuit to be circulated by using additional used dialysate. Therefore, the peritoneal dialysis process was automated by reinjecting the purified dialysate into the peritoneal cavity. Experiments were carried out continuously for a total of 4 hours and the concentration changes of the toxins and electrolyte were measured by sampling every 20 minutes.

Figure 4.27 showed the concentration change of body toxins (urea, creatinine) and electrolyte (Na^+, Cl^-) over time. The value was normalized by the initial injection concentration. In the case of urea, the concentration decrease of more than 80 % is steadily maintained except for the value measured at 200 minutes. In the case of creatinine, the concentration decrease of more than 50 % was stably maintained. It was because the creatinine adsorption performance of the filter stably supported the removal performance of the ICP device. In the case of Na^+, the concentration was decreased steadily by more than 30 % until 120 minutes, but it shake greatly

after 120 minutes. This instability was due to the instantaneous flow and voltage distribution imbalance as analyzed in the in-vitro test results. The concentration increase of urea after 120 min also be explained by the same conclusion. In the case of Cl^-, the concentration decrease tendency was lower than that of Na^+ since dialysate contained not only Na^+ but also various cationic species.

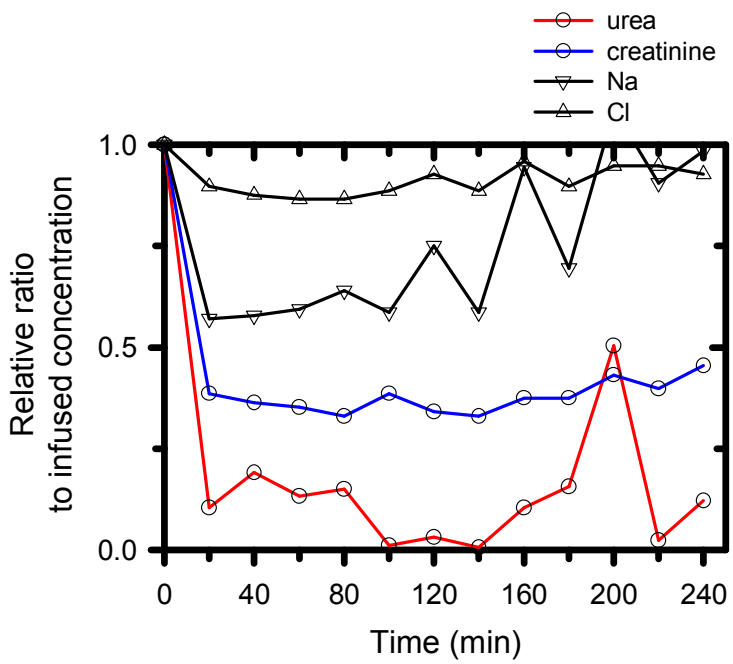

Figure 4.27: The normalized concentration change of body toxins (urea, creatinine) and electrolyte (Na^+, Cl^-) over time. The concentration of urea was decreased of more than 80 % except for moment of 200 minutes, creatinine was decreased of more than 50 %, and Na^+ was decreased steadily by more than 30 % until 120 minutes, but it fluctuated after 120 minutes.

The average removal rate of each component was shown in the following Figure 4.28. Urea showed an average removal rate of 83 %, creatinine 65 %, Na^+ 16 %, Ca^{2+} 40 %, P 30 % and Cl^- 7 %. Compared with the in-vitro test, the electric field was stably distributed so that urea was removed at a high removal rate, and creatinine was also stably removed due to the secondary performance of the filter. The reason why the average removal rate of sodium was low was because the minus removal rate was measured after 160 minutes and 200 minutes.

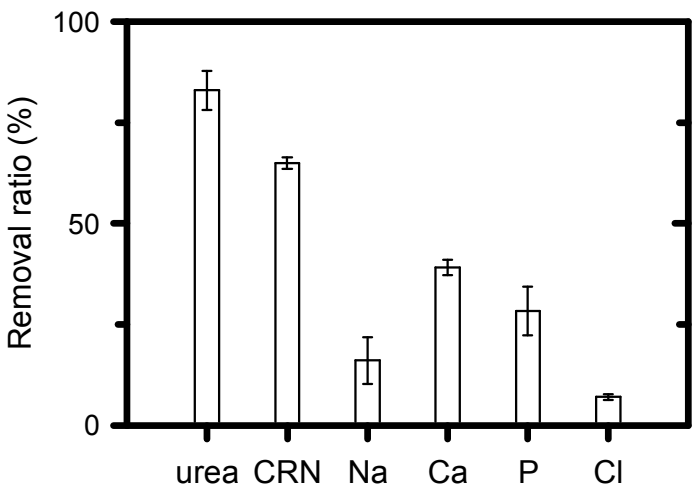

Figure 4.28: The average removal rate of each component in the used dialysate. Urea showed an average removal rate of 83 %, creatinine 65 %, Na^+ 16 %, Ca^{2+} 40 %, P 30 % and Cl^- 7 %.

Figure 4.29 showed the change in concentration of each component over time at the cathodic side chamber. The concentration values were normalized to the initial injection concentration values.

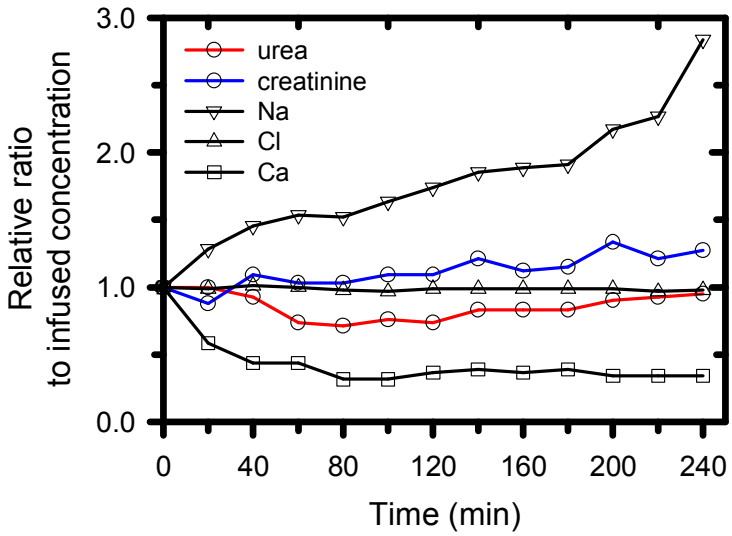

Figure 4.29: The normalized concentration change of each component over time at the cathodic side chamber. Creatinine and Na^+ showed gradual increase in concentration due to ICP phenomenon. Ca^{2+} showed a stable removal rate of more than 50 % in both anode and cathode chambers which meant precipitation by electric field.

Creatinine and Na^+ showed gradual increase in concentration since the components in the anodic side were transported to the cathodic side. In the case of Ca^{2+}, a stable removal rate of more than 50 % was observed in both anode and cathode chambers, so it would be predicted that precipitation by

electric field occurred. In the case of urea, it was analyzed that the decomposition did not occur at the anodic side chamber in the result of microchannel device. However, since the current value of this macro device was as high as 1 A level, interference between the anodic and cathodic side chamber would be occurred. Cl^- concentration was constant due to no migration through the nanoporous membrane.

The concentration change of the peritoneal dialysate in the peritoneal cavity of the beagle dogs, which was purified by ICP, was measured as shown in Figure 4.30. The concentration values were normalized to the initial injection concentration values. The concentration of urea was decreased steadily up to 90 minutes, but it was risen between 90 to 160 minutes and decreased again between 160 to 240 minutes. On the other hand, the creatinine concentration decreased until 40 minutes, but after that, it was higher than the initial concentration continuously. In the actual external circuit, urea was removed by 83 % and creatinine was 65 % so that purified dialysate was reinjected into the peritoneal cavity. However, since the exchange of the substance between the purified dialysate in the peritoneal cavity and the serum through the peritoneum occurs actively, urea and creatinine in the serum was newly diffused into the abdominal cavity. This amount of inflow was determined by the difference in the concentration of the substance in the serum and the substance in the peritoneal cavity so that such a non-uniform concentration distribution appeared. On the other hand,

Na^+ and Cl^- showed a stable concentration change because the mobility of ions was higher than that of the toxins and the mass exchange rate was fast.

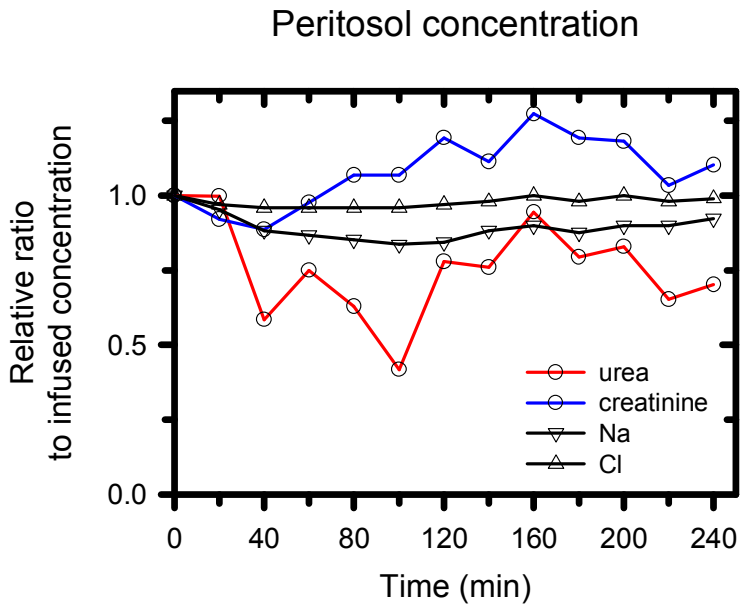

Figure 4.30: The normalized concentration change of the peritoneal dialysate in the peritoneal cavity of the beagle dogs. Although urea was removed by 83% and creatinine was 65 % by ICP purifier, the urea was not removed well even fluctuated, and creatinine was rather increased in concentration. This was because urea and creatinine in the serum was newly diffused into the abdominal cavity.

Figure 4.31 showed the change in serum concentration of beagle dog. The concentration values were normalized to the initial serum concentration values. As the purified dialysate was injected into the abdominal cavity, the

concentrations of urea, creatinine, Na^+ and Cl^- were gradually decreased with time. This was the evidence of the toxins removal process in the body fluids from the peritoneum by the purified dialysate. This results suggested that it was possible to replace the conventional peritoneal dialysis process in which new dialysate should be periodically exchanged by continuously purifying the dialysate with an ICP device. Therefore, ICP modules, pumps, filters, and sensors would be integrated to create portable artificial kidney which would be made commercially available.

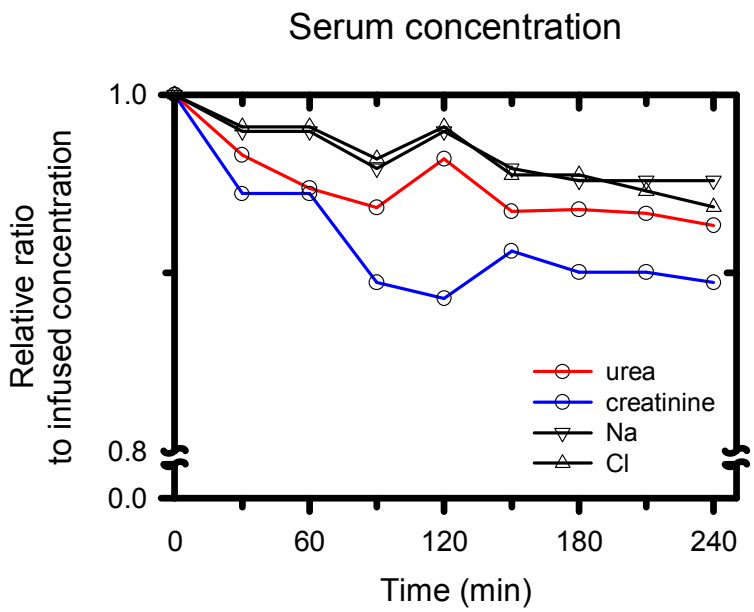

Figure 4.31: The normalized concentration change in serum of beagle dog. The concentrations of urea, creatinine, Na^+ and Cl^- were gradually decreased with time so that the toxins removal process in the serum from the peritoneum by dialysate purification by ICP.

Chapter 5 Conclusion

ICP has been reported as a versatile phenomenon for major industrial platform such as desalination and biomedical research field. However, its detailed (or exact) concentration of ions and analyte near the nanoporous membrane has been debated in split ways due to the limitation of direct experimental measurement. Extremely low-throughput of the micro/nanofluidic device would hinder a long-term sample collection. Here, instead of the direct measurement of collected sample, a concentration change in the prefilled sample was backwardly extracted by simple equations so that the concentration of individual ion in extremely low-throughput system was successfully measured without any experimental disturbances within short collection time. This method was applied to 9-branched micro-nanofluidic hybrid device having ~4 nL/min throughput through each branch, and concentration profiling of ion altered by ICP triggering was successfully measured. From these result, we clearly classified 3 regions formed by ICP; one for outside IDZ at the anodic side, and another for inside IDZ at the anodic side, and the last one for the IEZ at the cathodic side. As predicted by previous studies, most of charged species regardless of their polarity and size were rejected inside IDZ so that only ~5 % of both cation and anion were detected without any analyte molecules. Analytes larger than nanopore size regardless of their polarity rerouted their

path toward the outside IDZ so that the analytes were preconcentrated and simultaneously, only ~30 % of both cation and anion were left in the microchannel. We defined this concurrent process as “desalted analyte preconcentration”. Rest of ~65 % cation was transported across the nanojunction and anion was consumed by electrode reaction. These experimental verifications would be the key evidences to put an end of the argument for the trajectory of ions caused by ICP. Finally, this “desalted analyte preconcentration” process was applied to the novel concept of ink recycler. Undesirable salt was desalted (~60 % of salt remained) and simultaneously, ink molecules were preconcentrated (~200 %) without the loss of them in a single step operation. These results would be a key operation mechanism of various refinery industry such as biomedical and chemical industry. Furthermore, ion separation phenomenon was firstly discovered at the inside IDZ due to amplified electric-field causing non-negligible diffusioosmosis effect, and ion concentration ratio was highly enhanced at the IEZ by modulating the flow rate in the cathodic side.

As an application of concentration profiling results in Chapter 2, continuous dialysate recycler for peritoneal dialysis was successfully demonstrated using nanoelectrokinetic phenomenon including ICP in micro/nanofluidic format. We confirmed that the most of toxic substances were substantially removed. Charged substances such as Na^+, creatinine and albumin were electrically transported through nanojunction or repelled from

ion depletion boundary depending on their electrophoretic mobility, and electrically neutral substance such a urea was electrochemically decomposed. Moreover, we proposed the novel macrofluidic dialysate recycler using ICP phenomenon which significantly enhance the throughput. Although nanofluidic device with great performance has been actively developed for a decade, several impassable limitations of throughput still impeded commercial applications. The macrofluidic ICP recycler was demonstrated to have 0.3 mL/min of throughput with used dialysate (100 ~150 mM) at 30 V, ~30 % removal ratio as a result. Throughput and removal ratio would be regulated by leveraging electric conditions and pressure field. These results would be a key technology for chronic kidney disease patients to improve the quality of their life.

Bibliography

[1] L. Alvarado, A. C. Chen, *Electrochim Acta*, 2014, **132**, 583-597;

[2] H. Strathmann, *Desalination*, 2010, **264** (3), 268-288;

[3] M. E. Suss, S. Porada, X. Sun, P. M. Biesheuvel, J. Yoon, V. Presser, *Energ Environ Sci*, 2015, **8** (8), 2296-2319.

[4] T. Humplik, J. Lee, S. C. O' Hern, B. A. Fellman, M. A. Baig, S. F. Hassan, M. A. Atieh, F. Rahman, T. Laoui, R. Karnik, E. N. Wang, *Nanotechnology*, 2011, **22** (29).

[5] Probstein, R. F., *Physicochemical Hydrodynamics*: *An Introduction*, Wiley-Interscience, 1994.

[6] C. K. Chou, *Helping Water Managers Ensure Clean and Reliable Supplies.*, Lawrence Livermore National Laboratory, 2004.

[7] Fumatech GmbH (http://www.fumatech.com/EN/Membrane-processes /Process%2 Bdescription/Electrodialysis/index.html).

[8] GE Power Water & Process Technologies (http://www.gewater.com).

[9] A. B. Yaroslavtsev, V. V. Nikonenko, *Nanotechnologies in Russia*, 2009, **4**, 137-159.

[10] S. Schlumpberger, N. B. Lu, M. E. Suss, and M. Z. Bazant, *Environ. Sci. Technol. Lett.*, 2015, **2** (12), 367–372

[11] W. R. Walters, D. W. Weiser, L. J. Marek*, Industrial & Engineering Chemistry*,1955, **47**, 61-67.

[12] E. Laktionov, E. Dejean, J. Sandeaux, R. Sandeaux, C. Gavach, G. Pourcelly, *Separ Sci Technol*, 1999, **34** (1), 69-84.

[13] E. Korngold, L. Aronov, O. Kedem, *J Membrane Sci*, 1998, **138** (2), 165-170;

[14] R. Messalem, Y. Mirsky, N. Daltrophe, G. Saveliev, O. Kedem, *J Membrane Sci*, 1998, **138** (2), 171-180.

[15] K. H. Yeon, J. W. Lee, J. S. Lee, S. H. Moon, *J Appl Polym Sci*, 2002, **86** (7), 1773-1781.

[16] F. Dimascio, G. C. Ganzi, *Electrodeionization apparatus and method*, 1999, US5858191 A.

[17] G. C. Ganzi, F. Dimascio, A. J. Giuffrida, F. Wilkins, *Electrodeionization apparatus and method*, 1999, US 5868915 A.

[18] A. Grabowski, G. Q. Zhang, H. Strathmann, G. Eigenberger, *Sep Purif Technol*, 2008, **60** (1), 86-95.

[19] Siemens ED-CEDI desalination demo achieves 1.8 kWh/m³, Desalination & Water Reuse, 2011.

[20] E. Garcia-Quismondo, R. Gomez, F. Vaquero, A. L. Cudero, J. Palma, M. Anderson, *Phys Chem Chem Phys*, 2013, **15** (20), 7648-7656.

[21] I. Cohen, E. Avraham, Y. Bouhadana, A. Soffer, D. Aurbach, *Electrochim Acta*, 2015, **153**, 106-114.

[22] X. Gao, A. Omosebi, J. Landon, K. L. Liu, *Energ Environ Sci*, 2015, **8** (3), 897-909.

[23] S. I. Jeon, H. R. Park, J. G. Yeo, S. Yang, C. H. Cho, M. H. Han and D. K. Kim, *Energ Environ Sci*, 2013, **6** (5), 1471-1475.

[24] J. Lee, S. Kim, C. Kim and J. Yoon, *Energ Environ Sci*, 2014, **7** (11), 3683-3689.

[25] R. B. Schoch, J. Han and P. Renaud, *Rev. Mod. Phys*., 2008, **80**, 839.

[26] R. Austin, *Nat. Nanotech*., 2007, **2**, 79-80.

[27] J. C. T. Eijkel and A. Van Den Berg, *Microfluidics and Nanofluidics*, 2005, **1**, 249-267.

[28] S. M. Davidson, M. B. Andersen and A. Mani, *Phys. Rev. Lett*., 2014, **112**, 128302.

[29] T. Pundik, I. Rubinstein and B. Zaltzman, *Phys. Rev. E*, 2005, **72**, 061502.

[30] Q. Pu, J. Yun, H. Temkin and S. Liu, *Nano Lett*., 2004, **4**, 1099-1103.

[31] T. A. Zangle, A. Mani and J. G. Santiago, *Chem. Soc. Rev*., 2010, **39**, 1014-1035.

[32] S.-H. Lee, H. Lee, T. Jin, S. Park, B. J. Yoon, G. Y. Sung, K.-B. Kim and S. J. Kim, *Nanoscale*, 2015, **7**, 936-946.

[33] S. J. Kim, Y.-A. Song and J. Han, *Chem. Soc. Rev*., 2010, **39**, 912-922.

[34] S. J. Kim, Y.-C. Wang, J. H. Lee, H. Jang and J. Han, *Phys. Rev. Lett*., 2007, **99**, 044501.

[35] I. Cho, W. Kim, J. Kim, H.-Y. Kim, H. Lee and S. J. Kim, *Phys. Rev. Lett*., 2016, **116**, 254501.

[36] S. Nam, I. Cho, J. Heo, G. Lim, M. Z. Bazant, D. J. Moon, G. Y. Sung and S. J. Kim, *Phys. Rev. Lett.*, 2015, **114**, 114501.

[37] E. V. Dydek, B. Zaltzman, I. Rubinstein, D. S. Deng, A. Mani and M. Z. Bazant, *Phys. Rev. Lett*., 2011, **107**, 118301.

[38] D. Deng, E. V. Dydek, J.-H. Han, S. Schlumpberger, A. Mani, B. Zaltzman and M. Z. Bazant, *Langmuir*, 2013, **29**, 16167-16177.

[39] S. J. Kim, S. H. Ko, R. Kwak, J. D. Posner, K. H. Kang and J. Han, *Nanoscale*, 2012, **4**, 7406-7410.

[40] I. Rubinstein and B. Zaltzman, *Phys. Rev. E*, 2005, **72**, 011505.

[41] H. C. Chang, G. Yossifon and E. A. Demekhin, *Annual Review of Fluid Mechanics*, 2012, **44**, 401-426.

[42] V. V. Nikonenko, A. V. Kovalenko, M. K. Urtenov, N. D. Pismenskaya, J. Han, P. Sistat and G. Pourcelly, *Desalination*, 2014, **342**, 85-106.

[43] R. Kwak, G. F. Guan, W. K. Peng and J. Y. Han, *Desalination*, 2013, **308**, 138-146.

[44] S. H. Ko, Y. A. Song, S. J. Kim, M. Kim, J. Han and K. H. Kang, *Lab Chip*, 2012, **12**, 4472-4482.

[45] J. Choi, K. Huh, D. J. Moon, H. Lee, S. Y. Son, K. Kim, H. C. Kim, J.-H. Chae, G. Y. Sung, H.-Y. Kim, J. W. Hong and S. J. Kim, *RSC Advances*, 2015, **5**, 66178-66184.

[46] C.-H. Chen, A. Sakar, Y.-A. Song, M. A. Miller, S. J. Kim, L. G. Griffith, D. A. Lauffenburger and J. Han, *J. Am. Chem. Soc*., 2011, **133**, 10368-10371.

[47] S. Park, Y. Jung, S. Y. Son, I. Cho, Y. Cho, H. Lee, H.-Y. Kim and S. J. Kim, *Nat. Commun*., 2016, **7**, 11223.

[48] Y. Oh, H. Lee, S. Y. Son, S. J. Kim and P. Kim, *Biomicrofluidics*, 2016, **10**, 014102.

[49] S. H. Ko, S. J. Kim, L. Cheow, L. D. Li, K. H. Kang and J. Han, *Lab Chip*, 2011, **11**, 1351-1358.

[50] R. K. Anand, E. Heridan, K. N. Knust, and R. M. Crooks, *Anal. Chem.* 2011, **83**, 2351-2358.

[51] S. J. Kim, S. H. Ko, K. H. Kang and J. Han, *Nat. Nanotech*., 2010, **5**, 297-301.

[52] R. Kwak, S. J. Kim and J. Han, *Anal. Chem*., 2011, **83**, 7348-7355.

[53] K. N. Knust, D. Hlushkou, R. K. Anand, U. Tallarek and R. M. Crooks, *Angewandte chemie International Edition*, 2013, **52**, 8107-8110.

[54] G. Yossifon and H. C. Chang, *Phys. Rev. E*, 2010, **81**, 066317.

[55] C.-H. Chen, H. Lin, S. K. Lele and J. G. Santiago*, J. Fluid Mech*., 2005, **524**, 263-303.

[56] J. D. Posner and J. G. Santiago, *J. Fluid Mech.*, 2006, **555**, 1-42.

[57] C. L. Druzgalski, M. B. Andersen and A. Mani, *Physics of Fluids*, 2013, **25**, 110804.

[58] S. M. Rubinstein, G. Manukyan, A. Staicu, I. Rubinstein, B. Zaltzman, R. G. H. Lammertink, F. Mugele and M. Wessling, *Phys. Rev. Lett.*, 2008, **101**, 236101.

[59] B. Zaltzman and I. Rubinstein, *J. Fluid Mech*., 2007, **579**, 173-226.

[60] S. J. Kim, L. Li and J. Han, Langmuir, 2009, **25**, 7759-7765.

[61] R. Dhopeshwarkar, R. M. Crooks, D. Hlushkou and U. Tallarek, *Anal. Chem*., 2008, **80**, 1039-1048.

[62] K. A. Mauritz and R. B. Moore, *Chem. Rev.*, 2004, **104**, 4535-4585.

[63] J. H. Lee, Y.-A. Song and J. Han, *Lab Chip*, 2008, **8**, 596–601.

[64] H. Lee, J. Kim, H. Kim, H.-Y. Kim, H. Lee, S J Kim, *Nanoscale*, 2017, 10.1039/C7NR02075A.

[65] B. E. Conway, *Ionic hydration in chemistry and biophysics* (Elsevier Scientific Pub. Co., 1981).

[66] M. A. Silberberg, Chemistry 4th edition, *New York: McGraw-Hill*, 2006, pp. 431–434. ISBN 0-07-296439-1.

[67] S. Dhara, *Critical Reviews in Solid State and Materials Sciences*, 2007, **32** (1), 1–50.

[68] A. D. Adler; F. R. Longo; J. D. Finarelli; J. Goldmacher; J. Assour; L. Korsakoff;, 1967, *J. Org. Chem*., **32** (2), 476–476.

[69] Alan D. Adler; Frederick R. Longo; Frank Kampas; Jean Kim, *Journal of Inorganic and Nuclear Chemistry*, 1970, **32** (7), 2443.

[70] J. Dupont, C. S. Consorti, P. A. Z. Suarez, R. F. de Souza, *Organic Syntheses*, 2004, **10**, 184.

[71] S. R. Mikkelsen and E. Cortón, Bioanalytical Chemistry, *John Wiley & Sons*, Mar 4, 2004, pp. 247-267.

[72] "Plasmid DNA Separation: Fixed-Angle and Vertical Rotors in the Thermo Scientific Sorvall Discovery™ M120 & M150 Microultracentrifuges", ThermoFisherSCIENTIFIC.

[73] M. S. Bhamla, B. Benson, C. Chai, G. Katsikis, A. Johri, and M. Prakash, *Nat. Biomed. Eng*., 2017, **1**, 9.

[74] J. Crittenden, R. Trussell, D. Hand, K. Howe and G. Tchobanoglous, Water Treatment Principles and Design, 2nd edition, *John Wiley and Sons*. *New Jersey*, 2005, ISBN 0-471-11018-3.

[75] J. Glater, *Desalination*, 1998, **117**, 297–309.

[76] "Next Big Future: Israel scales up Reverse Osmosis Desalination to slash costs with a fourth of the piping", *nextbigfuture.com*, 2015.

[77] M. Clever, F. Jordt, R. Knauf, N. Räbiger, M. Rüdebusch, and R. Hilker-Scheibel, *Desalination*, **131** (1-3), 325–336.

[78] J.-M. Lain, D. Vial and P. Moulart, *Desalination*, 2000, **131**, 17-25.

[79] A. Bennett, *Filtration + Separation*, 2012, **49** (6), 28–33.

[80] R. H. Garrett, C. M. Grisham, Biochemistry 5th edition, *Belmont, CA: Brooks/Cole-Cengage Learning*, 2013, ISBN 9781133106296.

[81] J. Porath and P. Flodin, *Nature*, 1959, 1**83**(4676), 1657-1659.

[82] T. Sun, R. R. Chance, W. W. Graessley and D. J. Lohse, *Macromolecules*, 2004, **37**, 4304-4312.

[83] ThermoFisherSCIENTIFIC (https://www.thermofisher.com/kr/en/home /life-science/protein-biology/protein-purification-isolation/protein-dialysis-desalting-concentration.html/).

[84] Miller, S. A.; Dykes, D. D.; Polesky, H. F., *Nucleic Acids Res.,* 1988, **16** (3), 1215-1215.

[85] Health Insurance Review & Assessment Service (http://opendata.hira. or.kr/op/opc/olapMfrnIntrsIlnsInfo.do).

[86] S. S. A. Fenton, D. E. Schaubel, M. Desmeules, H. I. Morrison, Y. Mao, P. Copleston, J. R. Jeffery, and C. M. Kjellstrand, *Am. J. Kidney. Dis*., 1997, **30**, 334-342.

[87] W. Kim, K. Kim, H. Lee, Y. S. Kim, J. C. Lee, G. Y. Sung and S. J. Kim, MEMS, 2017 IEEE 30th International Conference on, Las Vegas, NV, USA, 10.1109/MEMSYS. 2017.7863405.

[88] A.C.S. Bezerra, E.L. de Sa, F.C. Nart, *J. Phys. Chem*. B 1997, **101**, 6443-6449.

[89] V.A. Gromyko, T.B. Tsygankova, V.B. Gaidadymov, Yu.B. Vasil'ev, V.S. Bagotskii, *Elektrokhimiya*, 1974, **10** (1), 57.

[90] V.A. Gromyko, T.B. Tsygankova, V.B. Gaidadymov, Yu.B. Vasil'ev, *Elektrokhimiya, 1975,* **11** (4), 589.

[91] W. Simka, J. Piotrowski, G. Nawrat, *Electrochimica Acta*, 2007, **52**, 5696–5703.

[92] K. Kim, W. Kim, H. Lee and S. J. Kim, *Nanoscale*, 2017, **9**, 3466-3475.

초록

지난 10여 년간 미세 공정 기술의 혁신적 발전과 함께 나노 수준의 공정을 포함한 미세 유체 장치 제작 기술 또한 발전해왔다. 이에 따라 기존에 수식으로만 널리 알려져 왔던 유체역학적 이론을 실험적으로 증명할 수 있게 되었고, 새로운 물리 현상 또한 발견되었다. 그 중 단연 흥미로운 현상은 이온 농도 분극 현상이라고 할 수 있다. 이온 농도 분극 현상은 나노막 주변에서 관찰되는 전기화학적 전달 현상으로 최근 10 여년동안 집중적으로 연구되어 오면서, 이론적인 나노전기동역학 연구뿐만 아니라 공학적 응용물 창출에도 많은 기여를 하고 있다. 하지만 나노막 내부에 대한 직접적인 관찰이 어렵기 때문에 간접적인 실험 증거와 함께 단일 이온 선택적 투과 특성 기원에 대한 논쟁이 여전히 진행중이다. 또한, 현재까지 개발된 이온 농도 분극 현상을 기반으로 하는 미세 유체 장치의 구조적 한계상 수처리 용량은 분당 nL 스케일 수준으로 실생활에 필요한 분당 mL 스케일 수준에 이르기까지에는 큰 무리가 따른다. 또한 수 mL의 샘플 양을 필요로 하는 질량분석기와 같은 정밀 측정 장비를 사용한 이온 농도의 측정이 어렵기 때문에, 나노막 양단에서 발생하는 이온 전달 기작에 대한 정량적 연구는 아직까지도 보고된 바 없으며, 전류 및 전도도 특성 분석만이 제공되고 있는 실정이다.

본 논문에서는 수학적 전략을 활용하여 아무리 작은 수처리 용량을 갖는 미세 유체 장치에서도 개별 이온 및 입자의 농도를 측정할 수 있는

정량적 농도 측정 방법을 제시하고, 이온 농도 분극 현상에 의하여 나노막 양단에서 발생하는 개별 이온의 전달 기작을 실험적으로 규명하였다. 그 결과, 이온 농도 분극 현상에 의하여 이온 공핍층 외부 영역과 내부 영역, 그리고 이온 증대층 이렇게 3가지 영역으로 크게 분류됨을 확인하였으며 이온 공핍층 외부와 내부의 전기적 중성 조건 충족을 위하여 농축과 탈염이 각기 다른 조건에서 진행될 것이라는 학계의 예상과 상반되는 새로운 실험적 증거들을 발견하였다. 먼저, 이온 공핍층 외부 영역에서는 분자량 500 이상의 분석물을 무손실 회수율로 농축함과 동시에 50 % 수준의 탈염이 동시에 이루어지는 프로세스를 발견하였다. 내부 영역에서는 기존에 보고된 것과 같이 탈염 및 정수 프로세스가 나타남을 확인하였으며, 이온 공핍층 내부에 유도되는 10^5 (V/m) 수준의 강한 전기장에 의하여 이온의 수화 셀이 벗겨지면서 리튬과 나트륨 이온의 농도 역전 현상이 일어남을 추가로 발견하였다. 이온 증대층에서는 나노막을 통한 양이온 이동이 65 %로 일어나기 때문에 개별 이온의 이동도 차이에 따른 농축과 함께 농도 증폭비 또한 조절할 수 있음을 보였다.

앞서 규명된 사실을 바탕으로 무손실 재생 잉크 제조 장치와 인공신장 개발을 위한 휴대형 연속 정화 장치, 2가지 응용물을 제안하였다. 기존 filtration 기술은 높은 탈염률을 보이지만, 분자량 500 수준의 잉크 분자에 대한 회수율이 상당히 낮기 때문에 액상 원료 기반 재생 잉크 제조 공정에서는 부적합하다. 하지만 이온 농도 분극 현상을 이용하면, 염 함유량이 높은 재생 잉크 원료를 무손실로 200 % 수준으로 농축함과 동시에 40 % 수준의 탈염을 단 한번의 프로세스로 동시에 달성 가능

함을 보였다. 마지막으로, 이온 농도 분극 현상에 의한 정수 기작을 활용하여 복막 폐투석액 내에 포함된 체내 독소 성분인 urea 및 creatinine의 제거 기작을 증명하였으며 연속 정화 시스템 구축이 가능함을 보였다. 실생활 사용을 위하여 0.1 uL/min 장치로부터 10 mL/min 장치까지 수처리 용량을 100,000 배 증대시킨 매크로 장치를 새롭게 선보이고, 체내 성능 테스트를 4시간 연속적으로 수행하여 혈중 독소 농도를 10 % 수준 감소 시킬 수 있음을 확인하였다. 본 결과를 활용하면, 기존의 정적 환경에서 진행되는 복막 투석을 대체할 수 있는 휴대형 인공신장을 개발할 수 있을 것으로 사료되며, 만성 신부전 환자의 삶의 질을 일반인 수준으로 끌어올 수 있을 것으로 기대된다.

Keywords : 마이크로 나노 유체 장치, 나노전기수력학, 이온 농도 분극 현상, 초미세 농도 측정, 동시 무손실 농축과 탈염, 휴대형 투석액 정화 장치

Student Number : 2013-30225